Journal of Controlled Release 392 (2026) 114699

Contents lists available at ScienceDirect

Journal of Controlled Release

journal homepage: www.elsevier.com/locate/jconrel

Engineered cargo-free nanoparticle decoys for phagocytic modulation of macrophages

Peyton M. Panovich [a], Aditi Ganesan [a], Arianna I. Markey [a], Miriam E. Stevens [a], Owen M. Kelly [a], Alexandra S. Piotrowski-Daspit [a,b,*]

[a] Department of Biomedical Engineering and Critical Care Medicine Division, University of Michigan Medical School, Ann Arbor, MI 48109, United States of America
[b] Department of Internal Medicine –Pulmonary and Critical Care Medicine Division, University of Michigan Medical School, Ann Arbor, MI 48109, United States of America

ARTICLE INFO

Keywords:
Nanoparticles
Gene delivery
Drug delivery
Mononuclear phagocytic system

ABSTRACT

Polymeric nanoparticles (NPs) are a versatile delivery platform for non-viral genetic therapies. However, a key shortcoming of polymeric NPs (and other non-viral delivery vehicles) is the often-high accumulation of NPs within the liver and the spleen after systemic intravenous (IV) administration *in vivo*. This phenomenon is largely the result of the mononuclear phagocytic system (MPS), a class of phagocytic cells responsible for native immune response and toxin clearance within the body. One strategy to overcome NP clearance by the MPS is the use of phagocytic modulating pre-treatments to intentionally and temporarily alter the phagocytic behavior of macrophages such that sequentially administered therapeutic NPs can be delivered to extrahepatic and extrasplenic tissues. Here, we explore the use cargo-free poly(lactic-*co*-glycolic acid) (PLGA) "decoy" NPs as pre-treatments for phagocytic evasion of sequentially administered therapeutic NPs. Analysis via flow cytometry and fluorescence microscopy reveal that cargo-free PLGA NPs significantly decrease uptake of subsequently administered therapeutic NPs by macrophages. Specifically, we conclude that variables such as size, surfactant composition, and timing of pre-treatment influence the behavior of cargo-free PLGA decoy NPs in modulating phagocytic activity of macrophages. In *in vivo* studies, we report decreased accumulation in the liver and increased deposition of therapeutic NPs in the lung with pre-administration of cargo-free decoy PLGA NPs. Together, these studies suggest pre-treatment with decoy NPs can reduce therapeutic NP clearance, with the potential to improve nanomedicine delivery capabilities for a wide range of therapeutics and disease targets.

1. Introduction

The transformative impact of non-viral nucleic acid delivery has been demonstrated recently by the COVID-19 lipid nanoparticle (LNP)-based vaccines as an intramuscular injection [1], the drug patisiran targeting hepatocytes in the liver [2], and pre-clinical data demonstrating gene editing *in vivo* mediated by CRISPR/Cas9 [3]. Like LNPs, polymeric nanoparticles (NPs) offer a promising alternative non-viral delivery platform for genetic therapies [4]. Poly (lactic-*co*-glycolic acid) (PLGA), for example, is a non-toxic, biodegradable, and already FDA-approved material for several drug delivery applications [4–7]. This polymer is widely used in the field of nanomedicine for both local and intravenous (IV) administration *in vivo* [8–11]. Additionally, we have developed poly(amine-co-ester)s (PACEs), which are a family of mildly cationic, biodegradable, and biocompatible polymers with high tunability and nucleic acid encapsulation efficiency [12–14]. PACE NPs are effective for the delivery of a wide range of nucleic acids such as plasmid DNA, mRNA, and siRNA both in cell culture and *in vivo* [4,13,15,16]. In the context of IV administration, however, a major barrier for non-viral delivery vehicles, including both polymeric NPs and LNPs, is the often-high and unintended accumulation of NPs in the liver and spleen when these are not the target tissues for disease therapeutics [4,6,7,11,17]. Indeed, the key challenge hindering widespread clinical application of non-viral genetic therapies remains precise delivery of these medicines in sufficient amounts to target tissues and cell types instead of non-target tissues [14].

Liver and spleen accumulation of NPs is largely the result of activity by the mononuclear phagocytic system (MPS) [18–20]. The MPS is a family of phagocytic cells including macrophages, dendritic cells, and phagocytes that are responsible for maintaining homeostasis in the

* Corresponding author at: 1600 Huron Parkway, Ann Arbor, MI 48109, United States of America.
E-mail address: asapd@umich.edu (A.S. Piotrowski-Daspit).

https://doi.org/10.1016/j.jconrel.2026.114699
Received 17 October 2025; Received in revised form 16 December 2025; Accepted 5 February 2026
Available online 9 February 2026

body, clearing foreign bodies from blood and tissues, and initiating immune responses [18]. Organs such as the liver and the spleen have large populations of phagocytic cells due to their filtration responsibilities. MPS cell populations include Kupffer cells in the liver and red pulp macrophages in the spleen, which contribute to the sequestration of NPs in these organs (Fig. 1A) [20–22]. Other physiological aspects contribute to this accumulation as well. For example, a large portion of the body's total blood volume is contained in the liver, resulting in high traffic to the fenestrated blood vessels in the organ for IV-administered therapeutics [23]. Additionally, a study by Tsoi et al. demonstrated that blood flow is significantly reduced in the liver sinusoid compared to other organ's capillaries, suggesting that there may be extended time for NP uptake in this tissue [24].

In addition to advances in NP design, strategies for MPS blockade

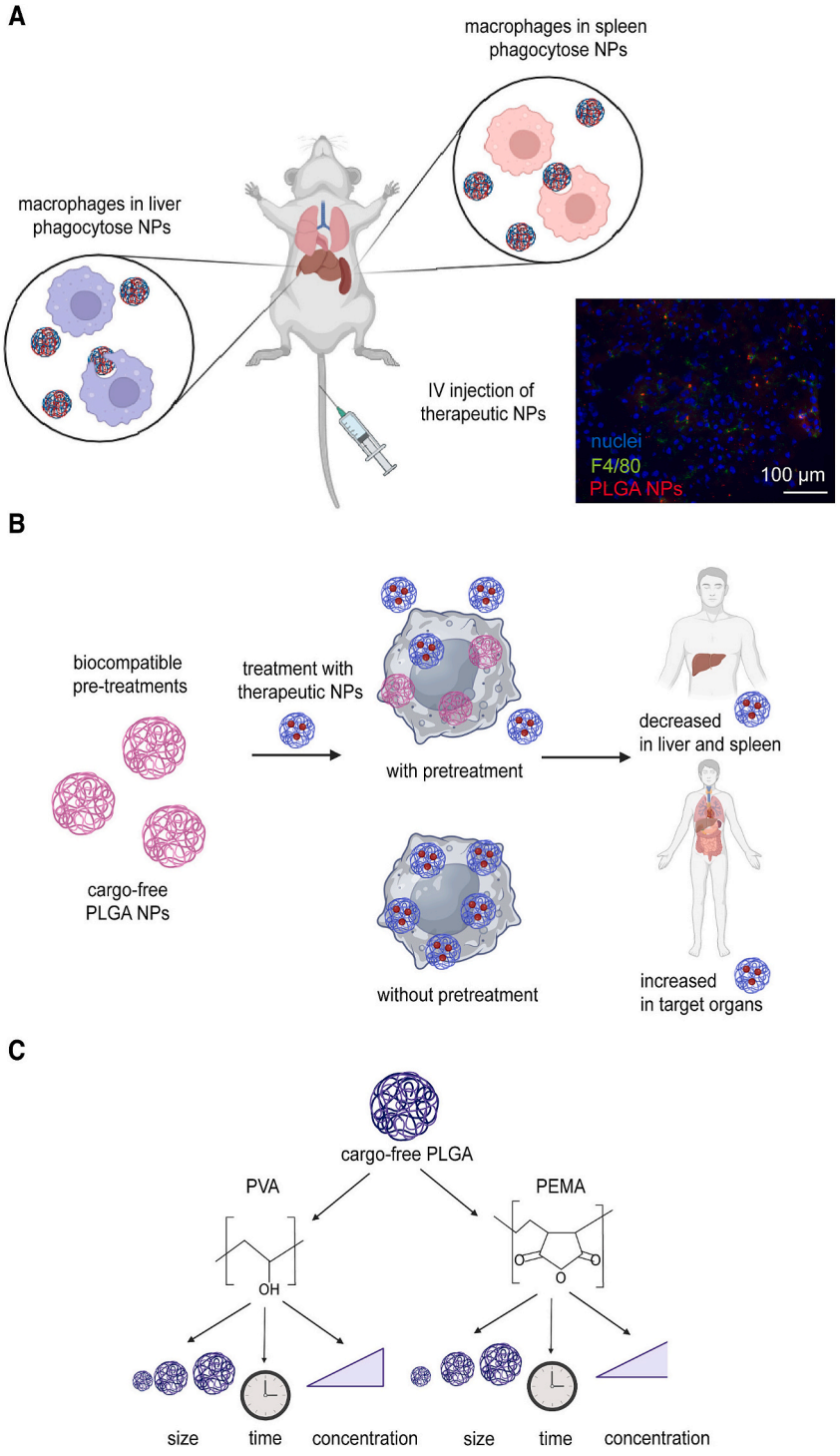

Fig. 1. A cargo-free PLGA decoy NP phagocytic modulation strategy. (A) Schematic of MPS cells in the liver and spleen clearing therapeutic polymeric NPs after IV injection *in vivo*. PLGA NPs co-localize with F4/80+ macrophages in the liver. (B) Schematic of the proposed mechanism of decoy NP-mediated phagocytic cell occupation; reducing clearance of subsequently administered therapeutic polymeric NPs by macrophages results in increased opportunities for NP accumulation in extrahepatic and extrasplenic target organs. (C) Schematic detailing parameters of interest for pre-treatment optimization in the present study. Schematics were prepared using BioRender.

have provided broad improvements to the therapeutic efficacy of non-viral nanomedicines. Typically, these strategies involve administration of a modulating agent to target MPS activity prior to IV administration of therapeutic NPs to achieve prolonged circulation time [25]. Different blocking agents can attenuate the activity of the MPS through distinct mechanisms. For example, clodronate liposomes are a strategy for macrophage suicide resulting in the physical depletion of phagocytic cell populations [14,20,25]. Tavares et al. demonstrate successful reduction of liver-resident Kupffer cells with pre-administration of clodronate liposomes [20]. While this strategy was found to be highly efficient for decreased delivery to hepatic tissues, depletion of phagocytic cells may have adverse effects on natural toxin clearance and immune responses in the body and is thus unlikely to be a viable strategy for clinical translation [26]. On the other hand, the strategy of temporary macrophage occupation prior to therapeutic NP administration, also referred to as MPS blockade, results in the temporary saturation of macrophages to decrease phagocytic clearance of subsequently administered therapeutics. Saturation would ideally be achieved using benign, biocompatible, and non-toxic molecules or biomaterials to ensure safety in a clinical setting. Pre-treatment with cargo-free lipid emulsions, liposomes, polymeric NPs, and anti-erythrocyte antibodies have already been shown to improve delivery of sequentially administered therapeutics to extrahepatic tissues *in vivo* [14,19,27,28]. Endocytosis prevention is another strategy that employs the use of molecular inhibitors to restrict the cell's ability to internalize foreign bodies [29,30]. Alternatively, macrophage shielding induces a physical barrier around the surface of the macrophage, blocking uptake of sequentially administered NPs. Other strategies include receptor saturation which occupies available endocytic receptors or gene regulation to downregulate the number of functional receptors [31,32]. However, the effects of these treatments on long-term macrophage viability and function are understudied. Moreover, exploration and optimization of pre-treatment administration parameters (timing, dose, material, etc.) are necessary for eventual clinical translation of a macrophage activity-modulating therapeutic enhancement strategy.

Cargo-free non-viral NPs themselves can serve as pre-treatment candidates by acting as "decoy" particles for intentional uptake in macrophages. For example, we have previously described the use of blank or unloaded PLGA NPs as a pre-treatment to therapeutic PACE NPs for MPS evasion *in vivo* [14]. We observed that IV pre-treatment with unloaded PLGA NPs promoted more widespread biodistribution of subsequently administered PACE NPs in mice. When PACE NPs were loaded with siRNA against proprotein convertase subtilisin/kexin type 9 (PCSK9), a protein that regulates the levels of low-density lipoprotein (LDL) [33], we found that blank PLGA NP pre-treatment significantly enhanced PCSK9 knockdown in hepatocytes and reduced blood cholesterol levels compared to PACE siRNA NPs administered without decoy NP pre-treatment [14]. The concept of unloaded polymeric NPs has also been explored outside of the context of nucleic acid delivery. For example, a study by Banka et al. describes the use of cargo-free polymeric NPs to decrease thrombo-inflammation by redirecting neutrophil-platelet aggregates away from sites of inflammation [34]. Cargo-free polymeric NPs have also been pre-administered to redirect immune cells for the improved efficacy of sequentially administered immunotherapies for the treatment of metastatic breast cancer [35]. Two surfactants commonly used to formulate PLGA NPs, polyvinyl alcohol (PVA) and poly (ethylene-*alt*-maleic anhydride) (PEMA), have been shown to induce different inflammatory responses [35,36]. Specifically, Casey et al. report that NPs formulated with PEMA result in an anti-inflammatory response compared to NPs formulated with PVA which tend to promote inflammation [36]. Pro/anti-inflammatory signals have direct correlation to macrophage polarization state where M1 macrophages are associated with pro-inflammatory cytokines while M2 macrophages are associated with anti-inflammatory cytokines [37]. M2 macrophages are considered more phagocytic than pro-inflammatory M1 macrophages suggesting that formulation surfactants may modulate the phagocytic behavior of MPS cells [38,39]. Together, these studies demonstrate the capability of therapeutic modulation by cargo-free NPs. However, variables such as timing of decoy administration, dosing, NP characteristics, and long-term effects can benefit from further study at the cellular level. Here, we investigate cargo-free PLGA NPs as pre-treatments for MPS evasion of sequentially administered therapeutic PLGA and PACE NPs (Fig. 1B). We employ cell culture studies for the exploration of multiple parameters on the phagocytic macrophages themselves (including primary cells) and their response to decoy pre-treatment (Fig. 1C) before validating our findings *in vivo*. We anticipate that the results presented in this study will be relevant to a wide range of therapeutic carriers including both LNPs and polymeric NPs and establish recommendations for future therapeutic applications.

2. Results

2.1. Pre-treatment with blank PLGA (PVA) decoy NPs reduces phagocytic clearance of therapeutic NPs in a size- and concentration-dependent manner

A major benefit of using unloaded/blank PLGA decoy NPs as a pre-treatment is that these vehicles are highly tunable during formulation, with the ability to modulate NP size [40]. Furthermore, PVA and PEMA can be interchanged as surfactants in the formulation process to achieve different vehicle properties [41]. We first tested cargo-free PLGA NP decoys formulated with PVA to determine the optimal size for use as a decoy pre-treatment. RAW 264.7 cells and primary bone marrow derived macrophages (BMDMs) from BALB/c mice were treated with 0.05 mg/mL of 200 nm, 300 nm, 400 nm, or 500 nm (hydrodynamic diameter as measured by dynamic light scattering (DLS)) cargo-free PLGA (PVA) decoys for 24 h (Table S1). Following cargo-free PLGA NP pre-treatment, the cells were treated with 0.05 mg/mL PLGA NPs loaded with DiIC18(5); 1,1′-dioctadecyl-3,3,3′,3′- tetramethylindodicarbocyanine, 4-chlorobenzenesulfonate salt (DiD) fluorescent dye as a surrogate for therapeutic NPs. Flow cytometry results indicated that pre-treatment with 500 nm cargo-free PLGA (PVA) decoys in RAW 264.7 cells significantly decreased the percent change in mean fluorescence intensity (MFI) compared to cells treated only with DiD NPs (Fig. 2A). This experiment was repeated in primary BMDMs where we also observed the lowest therapeutic clearance in cells pre-treated with 500 nm PLGA (PVA) NP decoys (Fig. 2E). Samples of the culture medium at time of administration and after 24 h were also collected and analyzed via fluorometry, as above. Here, we observed the highest fluorescence intensity in RAW 264.7 cells and primary BMDMs pre-treated with 500 nm cargo-free PLGA (PVA) NP decoys (Fig. 2B, F). Together, these data suggest that PLGA (PVA) decoys effectively decrease the phagocytic clearance of therapeutic NPs in both RAW 264.7 cells and primary BMDMs.

After determining the optimal size of cargo-free PLGA (PVA) NP decoys, we next sought to determine the optimal concentration for reduced phagocytic clearance. We varied the treatment concentration of 500 nm cargo-free PLGA (PVA) NP decoys between 0.1 mg/mL and 0.4 mg/mL in RAW 264.7 cells and primary BMDMs prior to treatment with DiD-loaded NPs as above. All PLGA (PVA) NP decoy concentrations resulted in significant reduction of phagocytic clearance in RAW 264.7 cells with no significant difference between results of experimental groups, suggesting that even low concentrations of decoy NPs are effective (Fig. 2C). Fluorescence quantification of the cell culture medium, however, suggests that 0.3 mg/mL treatment with PLGA NP decoys may provide slight improvement over the other concentrations (Fig. 2D). In primary BMDMs, we observed the lowest therapeutic NP clearance from cells pre-treated with 0.4 mg/mL 500 nm cargo-free PLGA (PVA) NP decoys (Fig. 2G). Fig. 2H supports these findings; we observed highest fluorescent signal remaining in the cell culture medium from cells pre-treated with 0.4 mg/mL 500 nm cargo-free PLGA (PVA) NP decoys. For experiments conducted in RAW 264.7 cells,

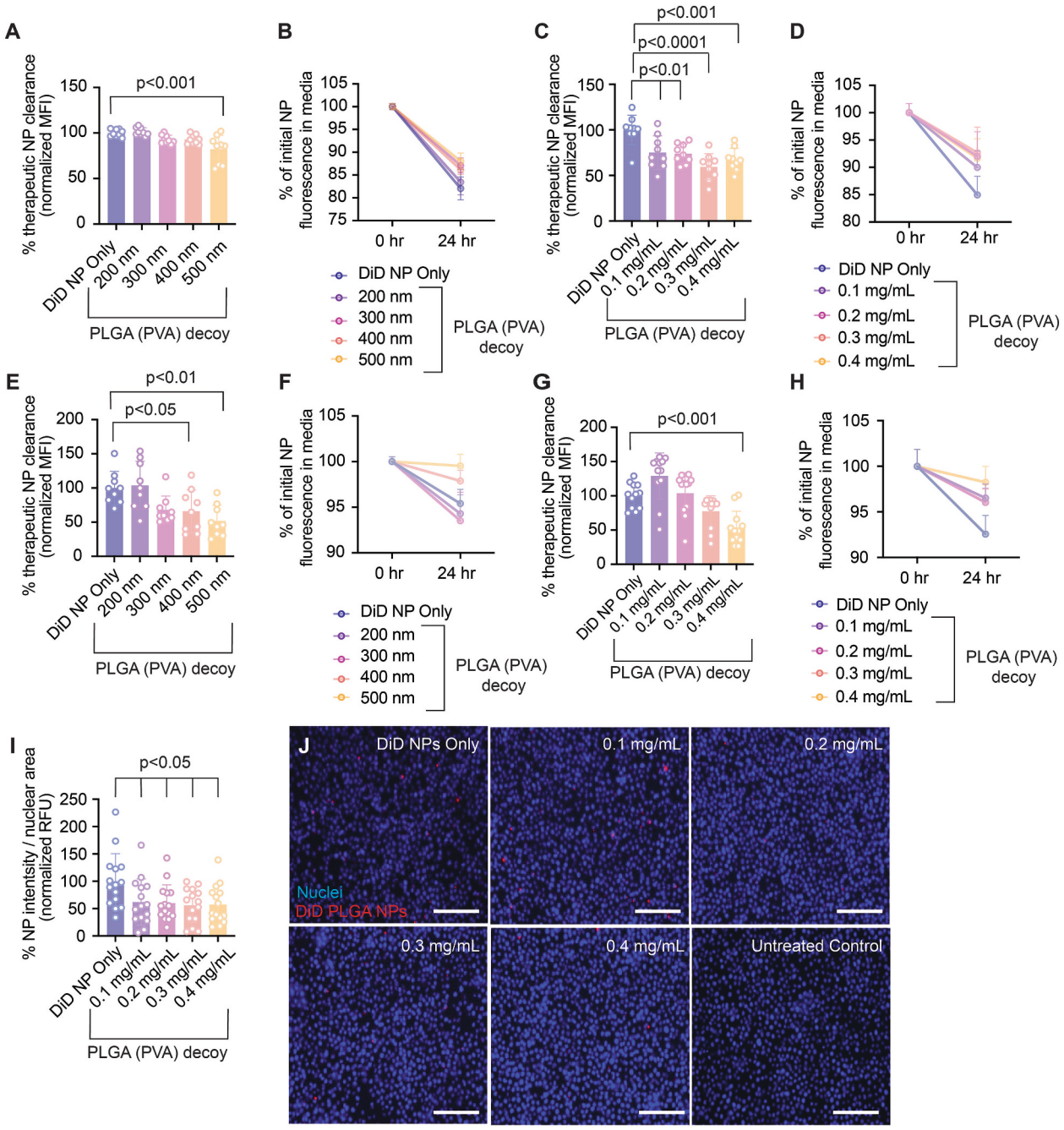

Fig. 2. Size and concentration of cargo-free PLGA (PVA) decoy NPs decrease phagocytic clearance of therapeutic PLGA NPs Percent therapeutic NP clearance (normalized MFI) of RAW 264.7 cells (A) or BMDMs (E) pre-treated with 0.05 mg/mL of 200, 300, 400, or 500 nm cargo-free PLGA (PVA) NP decoys followed by treatment with 0.05 mg/mL therapeutic DiD-loaded PLGA NPs ($n = 9$, error bars represent SD of mean). Percent initial NP fluorescence remaining in culture medium (normalized relative fluorescence intensity (RFU)) for fluorescent quantification of cell culture medium in RAW 264.7 cells (B) or BMDMs (F) pre-treated with 0.05 mg/mL of 200, 300, 400, or 500 nm cargo-free PLGA (PVA) NP decoys followed by treatment with 0.05 mg/mL therapeutic DiD-loaded PLGA NPs ($n = 9$, error bars represent SEM). Percent therapeutic NP clearance (normalized MFI) of RAW 264.7 cells (C) or BMDMs (G) pre-treated with 0.1, 0.2, 0.3, or 0.4 mg/mL 500 nm cargo-free PLGA (PVA) NP decoys followed by treatment with 0.05 mg/mL therapeutic DiD-loaded PLGA NPs ($n = 9$, error bars represent SD of mean). Percent initial NP fluorescence remaining in culture medium (normalized RFU) in RAW 264.7 cells (D) or BMDMs (H) pre-treated with 0.1, 0.2, 0.3, or 0.4 mg/mL 500 nm cargo-free PLGA (PVA) NP decoys followed by treatment with 0.05 mg/mL therapeutic DiD-loaded PLGA NPs (n = 9, error bars represent SEM). (I) Percent NP intensity normalized to nuclear area (normalized RFU) as calculated by MATLAB quantification of (H) fluorescence microscopy images of RAW 264.7 cells pre-treated with 0.1, 0.2, 0.3, or 0.4 mg/mL 500 nm cargo-free PLGA (PVA) NP decoys followed by treatment with 0.05 mg/mL therapeutic DiD-loaded PLGA NPs ($n = 15$, error bars represent SD of mean). Nuclei: blue, DiD-loaded PLGA NPs: red, scale bars: 150 μm. A one-way ANOVA with multiple comparisons was used for statistical analysis where experimental groups are compared to DiD NP only condition. (For interpretation of the references to colour in this figure legend, the reader is referred to the web version of this article.)

fluorescence microscopy images (Fig. 2J) further corroborate these findings; we observed the lowest NP signal for wells pre-treated with 0.3 mg/mL cargo-free PLGA (PVA) NP decoys. Finally, fluorescence intensity of therapeutic NPs per nuclear area was quantified in these images using a custom MATLAB code where results are reported as percent NP intensity normalized to nuclear area (Fig. S1) [17,42]. Fig. 2I depicts the results of this quantification, further supporting the lowest DiD signal from experimental groups pre-treated with 0.3 mg/mL cargo-free PLGA (PVA) NPs. However, no statistically significant differences were observed among experimental groups. Consequently, 0.2 mg/mL was selected for future studies as it achieved comparable results at a lower dose. Further, for experiments conducted in primary BMDMs, fluorescence microscopy images (Fig. S2B) and corresponding MATLAB quantification (Fig. S2A) reveal that cells pre-treated with 0.3 mg/mL 500 nm cargo-free PLGA (PVA) decoys is the optimal dosing for reduced clearance of therapeutic NPs.

2.2. Pre-treatment with blank PLGA (PEMA) decoy NPs reduces phagocytic clearance of therapeutic NPs

In addition to investigating PLGA (PVA) NP decoys, we also determined how PLGA NP formulation with PEMA as an alternative surfactant affects decoy efficacy. As above, we formulated unloaded PLGA (PEMA) NPs of various sizes (Table S1). We then pre-treated RAW 264.7 cells and primary BMDMs with 300 nm, 400 nm, 500 nm, or 600 nm (hydrodynamic diameter as measured by DLS) cargo-free PLGA (PEMA) decoy NPs. Analysis by flow cytometry revealed that RAW 264.7 cells pre-treated with 300 nm, 400 nm, or 600 nm cargo-free PLGA (PEMA) decoy NPs exhibited the largest decrease in phagocytic clearance of therapeutic NPs (Fig. 3A). These results were further verified by fluorescence quantification of cell culture medium; we observed the highest NP fluorescence intensity remaining in culture medium samples pre-treated with 300 nm PLGA (PEMA) NPs (Fig. 3B). In contrast to PLGA decoys formulated with PVA which exhibited a single optimal decoy size in RAW 264.7 cells, decoys formulated with PEMA exhibited less of a size dependence with multiple formulations resulting in significant decreased therapeutic NP clearance. This experiment was repeated in primary BMDMs, where we found that macrophages pre-treated with 400 nm PLGA (PEMA) NP decoys resulted in the lowest therapeutic NP clearance by flow cytometry (Fig. 3E). Fluorescence quantification of cell culture medium, however, revealed the highest remaining NP signal from cells pre-treated with 600 nm PLGA (PEMA) NP decoys (Fig. 3F). Discrepancies between these data collected via distinct modalities can likely be attributed to the larger range of error of the fluorometer. Consequently, we concluded that 400 nm PLGA (PEMA) NPs most consistently reduced phagocytic clearance as indicated by the lowest spread of data collected via flow cytometry in both cell lines.

Next, we determined the optimal concentration of cargo-free PLGA (PEMA) NPs to reduce phagocytic clearance of DiD-loaded therapeutic surrogate PLGA NPs. We pre-treated RAW 264.7 cells and primary BMDMs with 400 nm PLGA (PEMA) NP decoys at varying concentrations between 0.05 and 0.3 mg/mL prior to treatment with DiD-loaded therapeutic surrogate PLGA NPs. This range of concentrations is lower than that of experiments conducted with decoys formulated with PVA as cells pre-treated with cargo-free PLGA (PEMA) decoys were observed to have larger effects at the standard 0.05 mg/mL treatment when determining optimal size. Flow cytometry results revealed that RAW 264.7 cells pre-treated with 0.2 and 0.3 mg/mL of PLGA (PEMA) NP decoys resulted in significant decreases in therapeutic NP uptake (Fig. 3C). There was no significant difference between concentrations of 0.2 mg/mL and 0.3 mg/mL, which suggests that 0.2 mg/mL is sufficient for decoy pre-treatment. Fig. 3D depicts the fluorescence quantification of cell culture medium, which demonstrates similar trends we observed in the flow cytometry data. As above, this experiment was repeated in BMDMs, where we found that macrophages pre-treated with 0.3 mg/mL resulted in the lowest phagocytic clearance of therapeutic NPs (Fig. 3G, H). Finally, results were further verified by MATLAB quantification (Fig. 3I & S3A) of fluorescence microscopy images (Fig. 3J & S3B), which revealed the lowest percentage of DiD NP intensity normalized to nuclear area for experimental groups treated with 0.1 mg/mL and 0.3 mg/mL cargo-free PLGA (PEMA) NP decoys in RAW 264.7 cells and primary BMDMs, respectively. Combining results from flow cytometry and fluorescence quantification of cell culture medium, we conclude 0.2 mg/mL and 0.3 mg/mL as the optimal treatment concentrations of cargo-free PLGA (PEMA) NPs for experiments conducted in RAW 264.7 cells and primary BMDMs, respectively.

2.3. Timing and traffic patterns of cargo-free PLGA NP decoys

After observing differences in phagocytic clearance with different sizes, concentrations, and surfactants used for cargo-free PLGA NP decoys, we sought to determine whether there is an optimal timing of cargo-free PLGA NP decoy pre-administration. We also aimed to visualize the phagocytic uptake process for the cargo-free PLGA NP class of decoy. In this study, we treated RAW 264.7 cells with 300 nm PLGA (PVA) decoys encapsulating DiD for tracking via fluorescence signal. Although we determined 500 nm as the optimal size for PLGA (PVA) decoys, we used 300 nm in this microscopy study as the smaller particles allow for clearer visualization of NP trafficking patterns. Cell membranes were stained with the lipophilic dye Benzoxazolium, 3-octadecyl-2-[3-(3-octadecyl-2(3H)-benzoxazolylidene)-1-propenyl]-, perchlorate (DiO), and cell nuclei were stained with Hoechst 33342 for complete cell visualization. Fluorescence microscopy images were collected at 2-h increments between 2 and 12 h after treatment with DiD-loaded PLGA decoy NPs. We also collected images at 24 h post-treatment. Two hours after decoy administration, (Fig. 4B), we observed that the majority of decoy NPs remained in the culture medium outside of the cell. At 4 h post-treatment (Fig. 4C), PLGA decoy NPs begin concentrating around the cell membranes. Coating of the cell surface appears to occur between 6 (Fig. 4D) and 8 (Fig. 4E) hours post-treatment, as indicated by the arrow in Fig. 4D. At 10 h post-treatment (Fig. 4F), we observed decoy PLGA NPs beginning to enter the cytoplasm of the cells with more decoy NPs concentrating on the surface of the cells. Finally, it appears that at 12 h post-treatment (Fig. 4G), decoy PLGA NPs have begun to enter the perinuclear space with additional NPs saturating the surface of the cells. At 24 h post-treatment (Fig. 4H), we observe complete colocalization of NP signal with the cytoplasm and perinuclear space. Together, these images provide insight into the trafficking patterns and uptake behavior of cargo-free PLGA (PVA) decoy NPs in murine-derived macrophages.

2.4. Treatment duration of cargo-free PLGA (PVA/PEMA) decoy NPs affects phagocytic clearance of therapeutic PLGA NPs

Following the visualization of PLGA NP decoy uptake, we sought to quantify how decoy pre-treatment duration influences the phagocytic clearance of subsequently administered therapeutic NPs. Using similar procedures as above, we pre-treated RAW 264.7 cells with 0.2 mg/mL of either 500 nm PLGA (PVA) decoy NPs or 400 nm PLGA (PEMA) decoy NPs for a duration of 4–48 h. Fig. 5A and C depict flow cytometry results from RAW 264.7 cells reported in percent therapeutic NP clearance. In experiments where cells were pre-treated with PVA cargo-free PLGA NP decoys, treatment for 4 and 12 h resulted in the largest decrease in phagocytic clearance of therapeutic surrogate PLGA DiD NPs. For experiments in which cells were pre-treated with decoys formulated with PEMA, longer treatment times (12, 24, 36, and 48 h) resulted in the most significant evasion of phagocytic clearance. These results suggest that PEMA decoy efficacy may be correlated to a “phagocytic capacity” exhibited by the macrophages where the continued intracellular processing of decoy NPs may contribute more to the decreased clearance than cell surface saturation. This conclusion is further supported by the fluorescence analysis of cell culture medium (Fig. 5B, D), where we observe the highest fluorescence signal in the culture medium collected

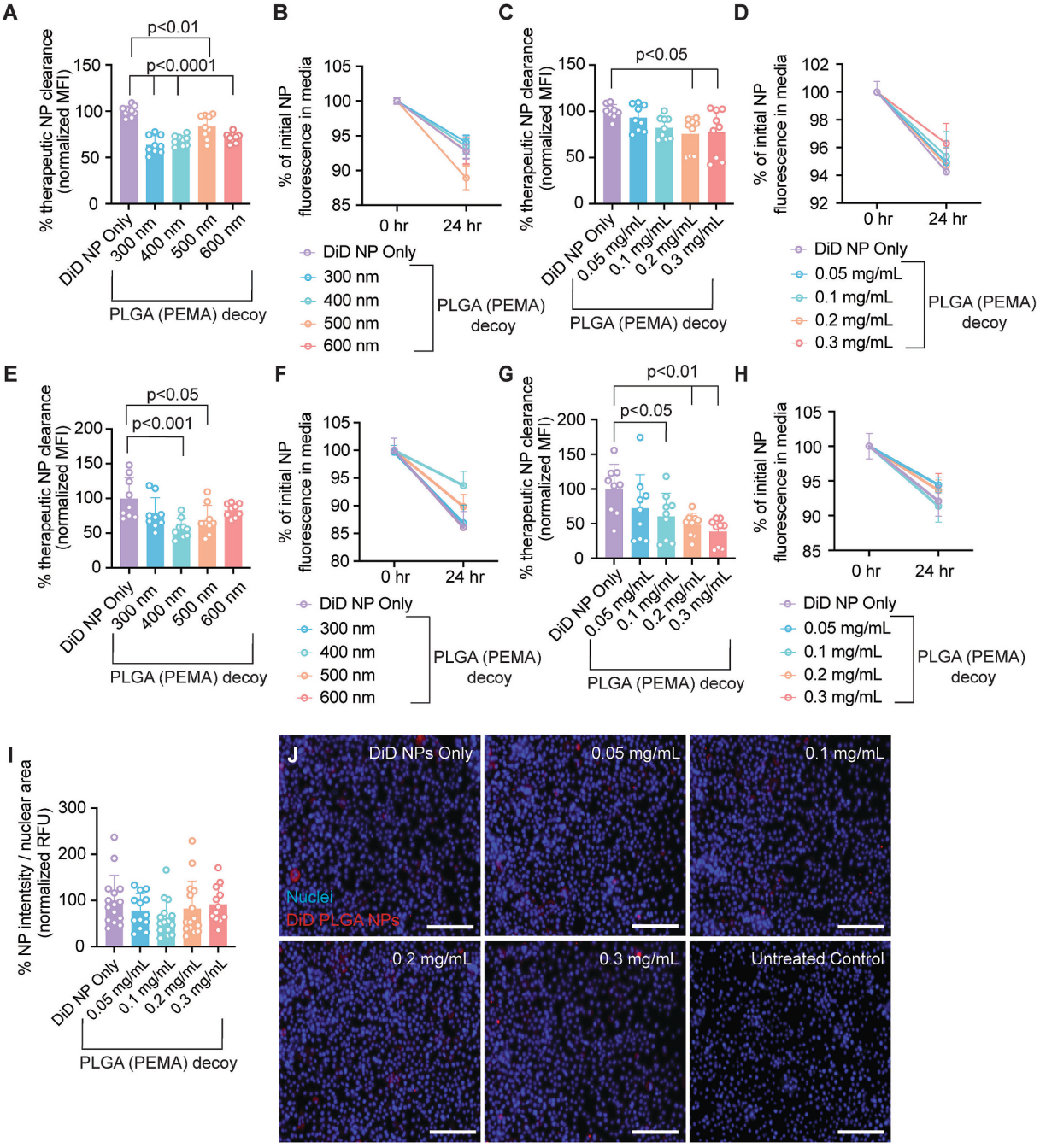

Fig. 3. Size and concentration of cargo-free PLGA (PEMA) decoy NPs decrease phagocytic clearance of therapeutic PLGA NPs Percent therapeutic NP clearance (normalized MFI) of RAW 264.7 cells (A) or BMDMs (E) pre-treated with 0.05 mg/mL of 300, 400, 500, or 600 nm cargo-free PLGA (PEMA) NP decoys followed by treatment with 0.05 mg/mL therapeutic DiD-loaded PLGA NPs ($n = 9$, error bars represent SD of mean). Percent initial NP fluorescence remaining in culture medium (normalized RFU) for fluorescent quantification of cell culture medium in RAW 264.7 cells (B) or BMDMs (F) pre-treated with 0.05 mg/mL of 300, 400, 500, or 600 nm cargo-free PLGA (PEMA) NP decoys followed by treatment with 0.05 mg/mL therapeutic DiD-loaded PLGA NPs ($n = 9$, error bars represent SEM). Percent therapeutic NP clearance (normalized MFI) of RAW 264.7 cells (C) or BMDMs (G) pre-treated with 0.05, 0.1, 0.2, or 0.3 mg/mL 400 nm cargo-free PLGA (PEMA) NP decoys followed by treatment with 0.05 mg/mL therapeutic DiD-loaded PLGA NPs (n = 9, error bars represent SD of mean). Percent initial NP fluorescence remaining in culture medium (normalized RFU) of fluorescent quantification of cell culture medium in RAW 264.7 cells (D) or BMDMs (H) pre-treated with 0.05, 0.1, 0.2, or 0.3 mg/mL 400 nm cargo-free PLGA (PEMA) NP decoys followed by treatment with 0.05 mg/mL therapeutic DiD-loaded PLGA NPs (n = 9, error bars represent SEM). (I) Percent NP intensity normalized to nuclear area (normalized RFU) as calculated by MATLAB quantification of (J) fluorescent microscopy images of RAW 264.7 cells pre-treated with 0.05, 0.1, 0.2, or 0.3 mg/mL 400 nm cargo-free PLGA (PEMA) NP decoys followed by treatment with 0.05 mL therapeutic DiD-loaded PLGA NPs ($n = 15$, error bars represent SD of mean). Nuclei: Blue, DiD-loaded PLGA NPs: red, scale bars: 150 μm. A one-way ANOVA with multiple comparisons was used for statistical analysis where experimental groups are compared to DiD NP only condition. (For interpretation of the references to colour in this figure legend, the reader is referred to the web version of this article.)

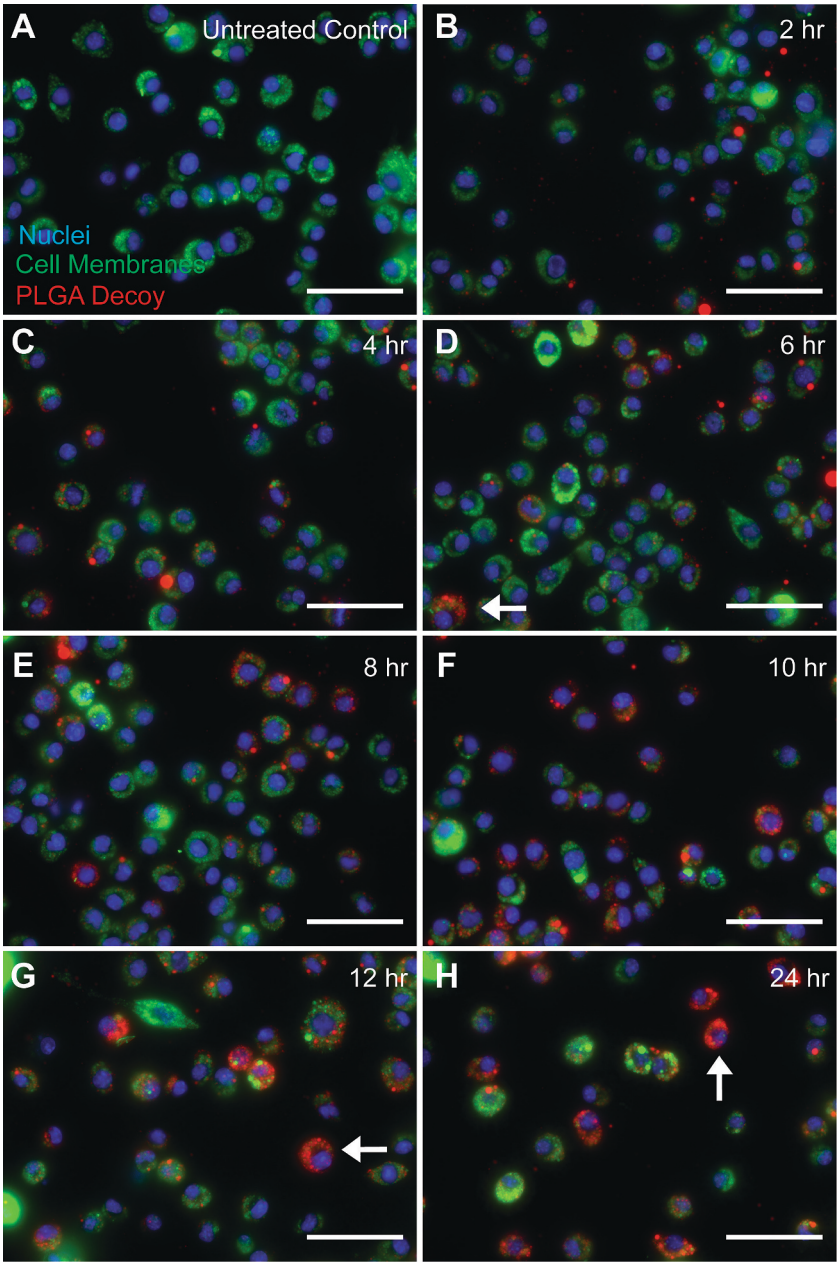

Fig. 4. Timing and traffic patterns of cargo-free PLGA NP decoys.
Fluorescence microscopy images of timepoint study of 300 nm DiD-loaded PLGA (PVA) decoy treatment on RAW 264.7 cells for (A) 2 h, (B) 4 h, (C) 6 h, (D) 8 h, (E) 10 h, (F) 12 h, or (G) 24 h. Nuclei: blue, cell membranes: green, DiD-loaded PLGA (PVA) decoys: red, scale bars: 75 μm.

from cells treated for 4 (PVA) and 48 h (PEMA). Statistically, however, we see no significant difference between the 24, 36, or 48-h experimental groups, suggesting that an efficiency plateau is met at the 24-h pre-treatment time for PEMA formulated cargo-free PLGA NPs according to flow cytometry results.

This experiment was repeated in primary BMDMs, however, cells were pre-treated with 0.3 mg/mL of the corresponding decoy. In experiments where cells were pre-treated with cargo-free PLGA (PVA) decoys, all treatment times were found to be statistically significant in decreasing phagocytic clearance; again, suggesting an efficiency plateau with duration of treatment time (Fig. 5E). Fluorescence quantification of cell culture medium revealed the greatest NP intensity remaining in the medium from cells pre-treated for 24 h (Fig. 5F). For experiments in which cells were pre-treated with cargo-free PLGA (PEMA) decoys, all treatment times were again found to significantly decrease clearance of therapeutic NPs (Fig. 5G). We observed the greatest fluorescence signal remaining in the culturing medium from groups pre-treated with cargo-free PLGA (PEMA) decoys for 8 h followed closely by those pre-treated for 36 h (Fig. 5H). Combining results from all data modalities, we conclude that 24 h is the optimal pre-treatment time for PVA decoys and 36 h is optimal for PEMA decoys used on primary BMDMs.

2.5. *Decoy pre-treatments are applicable to other NP delivery platforms*

In the studies discussed thus far, PLGA NPs have been used as a surrogate for therapeutic NPs. The field of NP-mediated drug delivery, however, expands far beyond PLGA with many delivery vehicles that are also subject to clearance by the MPS. Here, we demonstrate that decoy pre-treatments are also effective in evading phagocytic clearance of a class of PACE NPs formulated using the block *co*-polymer PACE-poly (ethylene glycol) (PACE-PEG). As above, RAW 264.7 cells were pre-treated with a survey of pre-treatments found to be most effective for

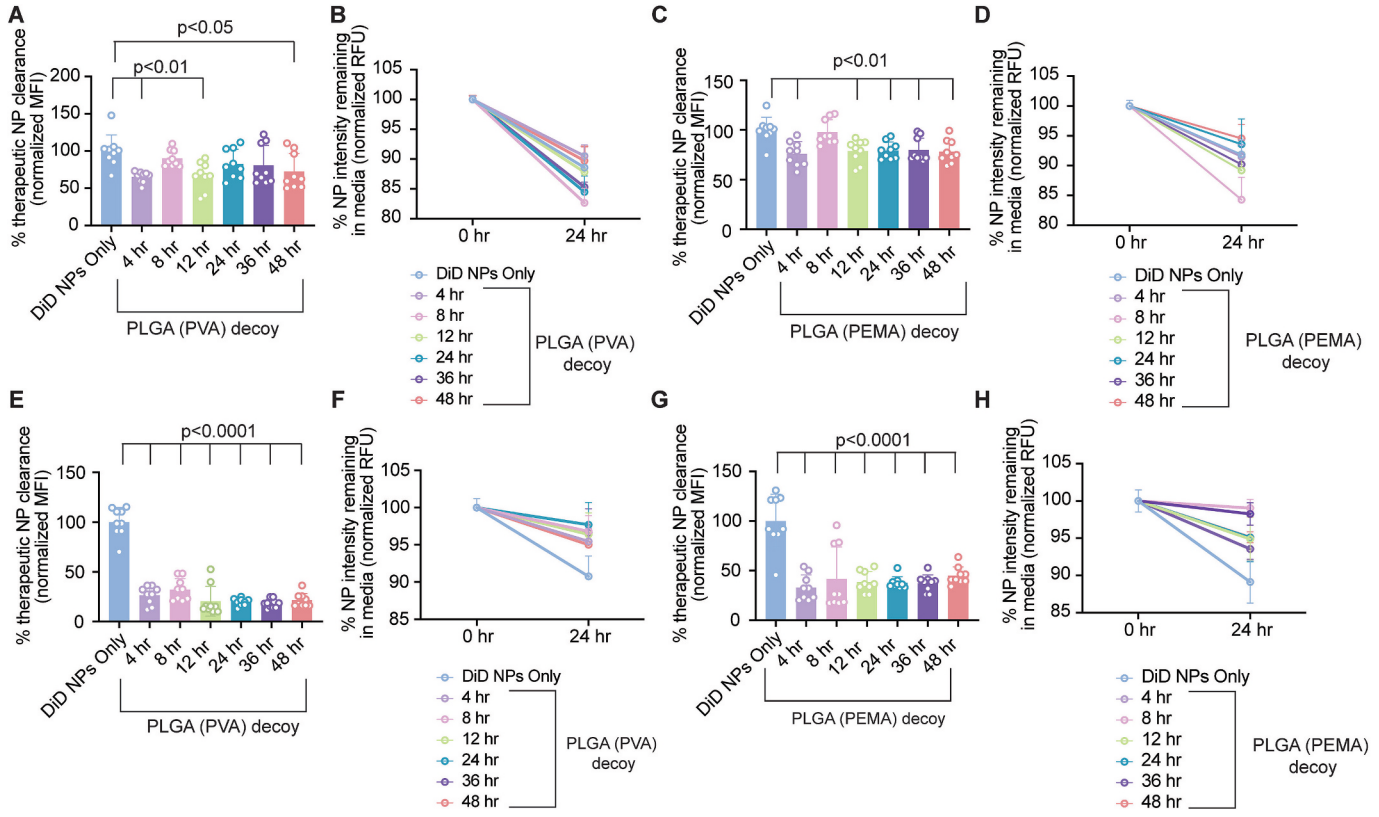

Fig. 5. Treatment time with cargo-free PLGA (PVA/PEMA) decoy NPs effect phagocytic clearance of therapeutic PLGA NPs Percent therapeutic NP clearance (normalized MFI) of RAW 264.7 cells pre-treated with 0.2 mg/mL (A) or BMDMs pretreated with 0.3 mg/mL (E) of 500 nm cargo-free PLGA (PVA) NP decoys for 4, 8, 12, 24, 36, or 48 h followed by treatment with 0.05 mg/mL therapeutic DiD-loaded PLGA NPs ($n = 9$, error bars represent SD of mean). Percent initial NP fluorescence remaining in culture medium (normalized RFU) in RAW 264.7 cells (B) or BMDMs (F) pre-treated with 500 nm cargo-free PLGA (PVA) NP decoys followed by treatment with therapeutic surrogate DiD-loaded PLGA NPs (n = 9). Percent therapeutic NP clearance (normalized MFI) of RAW 264.7 cells pre-treated with 0.2 mg/mL (C) or BMDMs pre-treated with 0.3 mg/mL (G) of 400 nm cargo-free PLGA (PEMA) NP decoys for 4, 8, 12, 24, 36, or 48 h followed by treatment with 0.05 mg/mL therapeutic surrogate DiD-loaded PLGA NPs (n = 9, error bars represent SD of mean). Percent initial NP fluorescence remaining in culture medium (normalized RFU) in RAW 264.7 cells (D) or BMDMs (H) pre-treated with of 400 nm cargo-free PLGA (PEMA) NP decoys followed by treatment with therapeutic DiD-loaded PLGA NPs (n = 9, error bars represent SEM).

reducing PLGA NP clearance (0.2 mg/mL 500 nm cargo-free PLGA (PVA) NPs and 0.2 mg/mL 400 nm cargo-free PLGA (PEMA) NPs). Following incubation with each pre-treatment, cells were treated with 0.1 mg/mL therapeutic surrogate PACE-PEG NPs loaded with DiD. Flow cytometry analysis revealed that both cargo-free decoy NP pre-treatments resulted in a decrease of PACE-PEG NP clearance. Experimental groups pre-treated with 500 nm cargo-free PLGA (PVA) NPs resulted in the most significant decrease compared to cells treated only with DiD-loaded PACE-PEG NPs (Fig. 6A). These results are further corroborated with fluorescence quantification of the cell culture medium, where we observed that experimental groups pre-treated with phagocytic modulators clustered at a higher remaining intensity compared to the DiD NP only control (Fig. 6B).

2.6. *Cargo-free PLGA NP decoys promote increased therapeutic deposition in the lung*

Finally, we sought to determine if our cell culture studies are representative of outcomes *in-vivo*. We formulated a library of PLGA NP decoys with DiD and therapeutic NPs with $DiIC_{18}(3)$; 1,1′-dioctadecyl-3,3,3′,3′-tetramethylindocarbocyanine) (DiI) for visualization of both decoy and therapeutic NP biodistribution (Table S2). BALB/c mice were administered a bolus 2 mg dose of each decoy formulation via retro-orbital (RO) injection; this dose was based on other reports of PLGA NPs administered IV [14,43]. Clodronate liposomes were administered at 2 mL/kg via RO injection as a positive control based on previous reports [14,20,43]. 24 h following decoy or clodronate liposome injection, mice were administered therapeutic surrogate NPs via RO injection to achieve a ~ 300 μg/mL blood NP concentration. Following a 24-h treatment with therapeutic NPs, mice were euthanized, and the heart, liver, lung, spleen, kidneys, and bone marrow were harvested from each animal. An In Vivo Imaging System (IVIS) was used to collect whole-organ fluorescence images of DiI-loaded therapeutic surrogate NPs in each organ. Fig. 7A,B depicts the whole-organ fluorescence images of therapeutic NPs and corresponding quantification. As anticipated, when mice are administered therapeutic NPs alone, we observed primary accumulation in the liver with no deposition in other tissue types. With pre-administration of decoy NPs, however, we observe a reduction of therapeutic NPs (as measured by fluorescence signal intensity) in the liver and increased deposition in the lung for all decoy formulations. Additionally, all decoy formulations achieved similar (if not improved) therapeutic NP deposition in the lung compared to clodronate liposome pre-administration.

Following IVIS imaging, organs (heart, liver, lung, spleen, kidneys, and bone marrow) were homogenized into single cell suspensions and analyzed via flow cytometry (Fig. 7C,D). Again, we observed primary accumulation of therapeutic NPs in the liver with limited signal found in extrahepatic tissues in animals that were administered therapeutic surrogate NPs only with no decoy pre-treatment. While we did not observe a decrease in the percentage of therapeutic surrogate NP positive cells in the bulk liver when animals are pre-administered PLGA NP decoys, we did observe increased therapeutic NP deposition in the lung. This is in

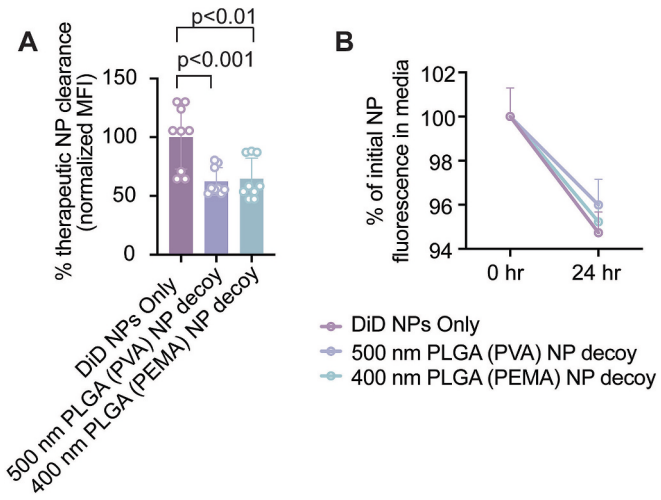

Fig. 6. Pre-treatments are applicable to other NP delivery modalities. (A) Percent therapeutic NP clearance (normalized MFI) of RAW 264.7 cells pre-treated with either 0.2 mg/mL 500 nm cargo-free PLGA (PVA) NP decoys, or 0.2 mg/mL 400 nm cargo-free PLGA (PEMA) NP decoys followed by treatment with 0.05 mg/mL therapeutic DiD-loaded PLGA NPs ($n = 9$, error bars represent SD of mean). A one-way ANOVA with multiple comparisons was used for statistical analysis where experimental groups are compared to DiD NP only condition. (B) Percent initial NP fluorescence remaining in culture medium (normalized RFU) in RAW 264.7 cells pre-treated with either 0.2 mg/mL 500 nm cargo-free PLGA (PVA) NP decoys, or 0.2 mg/mL 400 nm cargo-free PLGA (PEMA) NP decoys followed by treatment with 0.05 mg/mL therapeutic DiD-loaded PLGA NPs (n = 9, error bars represent SEM).

accordance with our previous study where we observed an increase in extrahepatic therapeutic delivery with no decrease in therapeutic liver deposition [14]; importantly, therapeutic NPs exhibited more widespread distribution throughout the liver instead of sequestration by F4/80$^+$ macrophages.

We further quantified the percent change in therapeutic surrogate NP MFI in the liver, spleen, and lungs (Fig. 7E-G). Decoy NPs formulated with PVA exhibited a larger percent decrease in MFI in the liver whereas decoy NPs formulated with PEMA exhibited a larger percent decrease of MFI in the spleen, suggesting that surfactant may influence biodistribution and clearance. Additionally, we observed that decoy NP size may result in more significant changes in MPS evasion in decoys formulated with PVA compared to PEMA. We observe that distinct decoy formulations (ex. 400 nm PLGA (PVA) NPs) result in optimal performance whereas decoys formulated with PLGA (PEMA) NPs of various sizes result in relatively similar outcomes. The same phenomenon was observed in cell culture where we observed that 500 nm PLGA (PVA) decoys resulted in the most pronounced phagocytic evasion whereas several PLGA (PEMA) decoys resulted in phagocytic evasion. Fig. 7H depicts the percent change in therapeutic surrogate NP positive cells in the lung where we noted a significant increase in percent positive cells in animals that were pre-administered 400 nm PLGA (PVA) NP decoys. Notably, we also report significant increases in both the percent change in MFI in the lung (Fig. 7G) and the percent change in therapeutic surrogate NP positive cells in the lung (Fig. 7H) in mice pre-treated with 400 nm PLGA (PVA) NP decoys compared to mice that received clodronate liposome pre-treatment, suggesting that cargo-free PLGA NP decoys can achieve improved MPS evasion without the depletion of MPS cells. Further, we found that there is both a significant increase in therapeutic NP positive cells in the lung following pre-treatment with PLGA (PVA) NP decoys and a significant increase in the amount of therapeutic surrogate NPs that each lung cell is internalizing.

Lastly, a portion of harvested livers and lungs were sectioned and imaged via fluorescence microscopy. Fig. 7J depicts a liver section from a mouse that was administered only therapeutic NPs and no decoys. In this case, we observed that therapeutic NPs (depicted in red) co-localize with F4/80+ phagocytic cells (depicted in green), suggesting that these NPs are readily phagocytosed and cleared from circulation without decoy NP pre-treatment. However, when mice are administered 400 nm PLGA (PVA) decoy NPs, we observe a broader deposition of therapeutic NPs suggesting that the pre-administered decoy NPs modulate the phagocytic cells in the liver resulting in evasion of phagocytosis by therapeutic NPs (Fig. 7K). Images of liver sections are complemented with lung sections where we observe minimal therapeutic NP delivery to the lung in the absence of decoy NP pre-treatment and substantially increased therapeutic NP deposition in mice pre-treated with 400 nm PLGA (PVA) decoy NPs (Figs. 7 M,N).

3. Discussion and conclusions

In the studies described above, we explore the use of cargo-free PLGA NPs as decoy pre-treatments to promote MPS evasion of subsequently administered therapeutic surrogate NPs. We first focused on the effects of cargo-free PLGA NP pre-treatments on the behavior of phagocytic cells in culture. These studies allowed us to focus on the behavior of a single cell type (including primary cells) responsible for phagocytic clearance in response to a wide range of conditions. Previously, we have demonstrated that PLGA NP decoys and therapeutic PACE NPs primarily co-localize with F4/80+ cells in the liver *in vivo,* further emphasizing the necessity for an in-depth exploration of phagocytic modulators in macrophages specifically [14]. In this study, we explored the effects of variables such as of size, concentration, surfactant composition, and duration of administration of cargo-free decoy PLGA NPs on phagocytic behavior. While these cell culture experiments informed design parameters of decoy NPs to be used *in vivo*, it is important to point out that some decoy formulations resulted in small differences in therapeutic surrogate NP clearance compared to cells treated only with therapeutic surrogate NPs. This is likely due to the limitations of cell culture experiments where excess NPs remain confined to the local environment during treatment. As NPs are readily internalized by macrophages, it is likely that all decoy NPs as well as the therapeutic NPs induced some form of macrophage saturation in these conditions, necessitating the evaluation of decoy NP efficacy in the *in vivo* environment.

The proof-of-concept *in vivo* studies presented here confirm the general trends reported from our cell culture experiments. For example, in cell culture, we report that larger PLGA (PVA) NP decoys result in a more substantial decrease in phagocytic clearance of therapeutic surrogate NPs. In our *in vivo* experiments, we similarly observed a significant increase in therapeutic NP deposition in the lungs in mice pre-treated with 400 nm PLGA (PVA) NP decoys. Further, in cell culture experiments, we report that PLGA NP decoys formulated with PEMA exhibit less of a size dependency in the context of phagocytic modulation; 300, 400, and 600 nm PLGA (PEMA) NP decoys performed similarly in terms of decreasing phagocytic clearance of therapeutic surrogate NPs. A similar trend was observed *in vivo* where we observed a 2-fold increase in therapeutic surrogate NP accumulation in the lungs for all PLGA (PEMA) decoy NP formulations. Together these data suggest that assessment of NP phagocytosis by macrophages in cell culture do provide predictive value for outcomes *in vivo*. Additionally, our *in vivo* results are relevant to pulmonary non-viral gene delivery for various lung pathologies [44]. For example, cystic fibrosis (CF) is characterized by mutations in the cystic fibrosis transmembrane conductance regulator (CFTR) gene encoding for a chloride channel [45,46]. Non-viral delivery of CFTR mRNA or gene editing technologies designed to ameliorate non-functional CFTR mutations have the potential to be curative [11,45,46]. Previously, we have demonstrated partial restoration of CFTR function with IV administration of peptide nucleic acid (PNA) NPs composed of PLGA to correct the F508del CFTR mutation [11]. A remaining hindrance of such approaches is therapeutic NP loss due to MPS activity, limiting therapeutic delivery to the lung — a

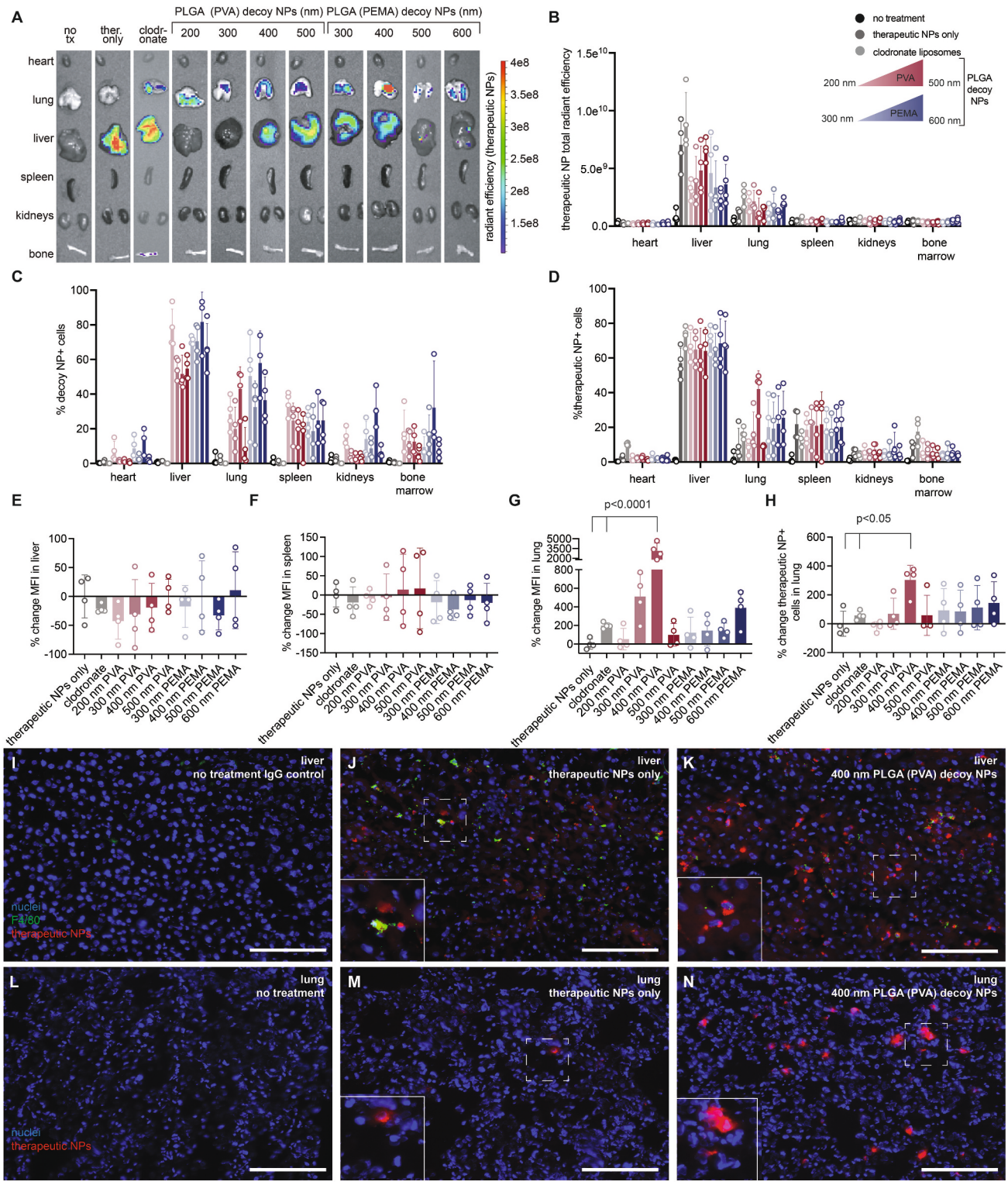

Fig. 7. Cargo-free PLGA NP decoys decrease sequestration of therapeutic NPs by macrophages in the liver *in vivo*. Representative whole-organ IVIS fluorescence images of DiI-loaded therapeutic NPs (A). Corresponding IVIS quantification for therapeutic surrogate NP (DiI) signal reported as total radiant efficiency (B). Percent cells positive for DiD-loaded PLGA decoy NPs (C) or DiI-loaded therapeutic surrogate NPs (D) in the heart, liver, lung, spleen, kidneys, and bone marrow from mice pretreated with clodronate liposomes, PLGA (PVA) decoy NPs (200–500 nm), or PLGA (PEMA) decoy NPs (300–600 nm) (D). Percent change in MFI in the liver (E), spleen (F), and lung (G) in mice pre-treated with clodronate liposomes, PLGA (PVA) decoy NPs (200–500 nm), or PLGA (PEMA) decoy NPs (300–600 nm). Percent change in therapeutic surrogate NP (DiI)-positive cells in the lung in mice pre-treated with clodronate liposomes, PLGA (PVA) decoy NPs (200–500 nm), or PLGA (PEMA) decoy NPs (300–600 nm) (H). Fluorescent microscopy images of liver sections from mice that received no treatment and stained with IgG control (I), mice treated only with therapeutic surrogate NPs (J), and mice pre-treated with 400 nm PLGA (PVA) decoy NPs (K). Fluorescent microscopy images of lung sections from mice that received no treatment (L), therapeutic surrogate NPs only (M), or mice pre-treated with 400 nm PLGA (PVA) decoy NPs (N). Nuclei: blue; F4/80: green; DiI-loaded therapeutic surrogate NPs: red.; scale bars: 100 μm. (For interpretation of the references to colour in this figure legend, the reader is referred to the web version of this article.)

challenge that could be overcome with decoy NP pre-treatment. Other pulmonary diseases such as chronic pulmonary obstructive disease (COPD), lung cancer, asthma, and interstitial lung disease (ILD) could also benefit from non-virally delivered genetic therapies enhanced by decoy NP pre-treatment [44].

The data presented above focus primarily on the use of PLGA NPs as therapeutic surrogate NPs. The field of polymeric NPs, however, is rapidly growing with new advances in synthetic polymer materials and NP formulation techniques. For example, the broader family of PACE NPs and poly (beta-amino ester) (PBAE) NPs are additional polymeric delivery vehicles that are designed for nucleic acid delivery [13,47–50]. These vehicles also have the potential to benefit from the use of decoy NPs to improve biodistribution *in vivo*. For example, we have shown that the use of cargo-free PLGA NPs as decoy pre-treatments can enhance siRNA delivery via PACE NPs [14]. In the present study, we observed efficient decoy NP activity with a 24-h pre-treatment duration of PLGA (PVA) NP decoys *in vivo*, which significantly decreased therapeutic NP clearance in BMDMs as outlined in our cell culture studies above. This suggests that the data presented here are likely to be applicable across multiple therapeutic NP delivery platforms.

As we have demonstrated, variables in NP formulation such as size and surfactant properties have significant influence on tissue tropism. As both decoy and therapeutic NP formulations can be modified for specific delivery outcomes, we believe that there is potential to optimize coupled decoy and therapeutic NP treatments for specific applications. In this study, we found that 400 nm PLGA (PVA) NP decoy pre-treatment resulted in the most significant deposition of 200 nm PLGA therapeutic surrogate NPs in the lung. It is important to note, however, that different therapeutic NP formulations (varying in chemistry, size, and surface charge) can result in different biodistribution patterns due to variations in natural tissue tropism. For example, while we did not show significant therapeutic deposition in tissues other than the lung with decoy NPs in this proof-of-concept study, it is likely that further optimization (ex. different polymer chemistries and NP properties) of both decoy NPs and therapeutic NPs could be used to achieve targeted delivery to other tissue types. Combining both our previous findings with PACE NPs [14], our current findings with PLGA NPs, and reports from LNP studies [27] we anticipate that cargo-free PLGA NP decoys will be widely applicable to many non-viral delivery platforms with the potential to benefit viral delivery modalities as well.

Overall, safety and biocompatibility of phagocytic modulators remain paramount to eventual clinical translation. PLGA is regarded as a generally safe biomaterial and has already received FDA approval for several drug delivery applications [51]. While the data presented in this study may not fall under the current applications for approval, the biodegradability and favorable safety profile of this polymer bode well for eventual translation [4,5,52]. The *in vivo* experiments in this study were performed with a 2 mg bolus PLGA NP decoy dose based on previous reports of PLGA NPs similar in size and characteristics administered to disease model animals [43] that were well-tolerated for multiple doses. This dose for our proof-of-concept study was chosen purposefully to ensure macrophage saturation in the liver. Future studies should include a decoy NP dose titration to determine the minimal dose of decoy NPs needed to achieve the desired delivery outcome. Careful dose conversion will be of utmost importance for future clinical translation. In summary, we are optimistic for future therapeutic applications of modulatory decoy NP pre-treatments to mitigate phagocytic activity to the broader field of nanomedicine.

3.1. Materials

RAW 264.7 cells (TIB-71) were purchased from the American Type Culture Collection (ATCC), Manassas, VA. Dulbecco's Modified Eagle's Medium (DMEM) (SH30023FS), high glucose DMEM (11965118), Hank's balanced salt solution (HBSS) (14–175-095), and Roswell Park Memorial Institute (RPMI) medium (11875093) were purchased from Gibco, Grand Island, NY and used as received. Fetal Bovine Serum (FBS) (SH3007103HI) and penicillin streptomycin (SV30010) were purchased from Cytiva, Marlborough, MA. Red blood cell lysis buffer (AAJ62150AK), Ultrapure water (10977023), and optimal cutting temperature (OCT) (4585) were purchased from ThermoFisher Scientific, Waltham, MA. Trehalose (BP268725) was diluted to 5 mg/mL in Ultrapure water and purchased from ThermoFisher Scientific. Goat serum (16210072) was diluted to 10% (*v*/v) in Dulbecco's phosphate buffered saline (DPBS) and purchased from ThermoFisher Scientific. Bovine serum albumin (BSA) (A7906), dichloromethane (DCM) (D65100), ethylenediaminetetraacetic acid (EDTA) (EDS-500G), and DNAse I (DN25-5G) were purchased from Millipore Sigma, Burlington, MA and used as received. PVA (36170) was diluted in Ultrapure water at 5% (*w/v*) and PEMA (188050) was diluted in Ultrapure water at 1% (w/v). Hoechst 33342 (5117) was diluted to 10 mg/mL in dimethyl sulfoxide (DMSO) and purchased from Tocris Bioscience, Bristol, UK. PLGA (B60101-2P) was purchased from Lactel Polymers, Birmingham, AL and used as received. Recombinant Murine Macrophage Colony Stimulating Factor (rM-MCSF) (ab129146) was diluted to 10 μg/mL in Ultrapure water and purchased from Abcam, Waltham, MA. DiD (D7757) was diluted in DMSO to 10 mg/mL and was purchased from Invitrogen, Waltham, MA. DiO (60011) and DiI (60010) was diluted to 10 mg/mL in DMSO and purchased from Biotium, Fremont, CA. PE anti-mouse F4/80, clone BM8 (123110), Zombie Green Viability Kit (423111), and anti-mouse F4/80, clone BM8 primary antibody (123102) was purchased from BioLegend, San Diego, CA, and used as received. Collagenase 1 (NC9096128) was purchased from Worthington Biochemical, Lakewood, NJ as used as received. Rat IgG isotype control (31933) and Alexa-fluor 488 goat anti-mouse IgG (A11001) were purchased from Invitrogen. Vectashield mounting medium (*H*−2000−10) was purchased from Vector Laboratories, Newark, CA and used as received. Clodronate liposomes (CLD8909). were purchased from Encapsula Nanosciences, Brentwood,TN and used as received.

4. Methods

4.1. Cell culture

RAW 264.7 cells were cultured in DMEM fortified with equal parts Ham's F-12 medium and completed with 10% (*v*/v) FBS and 1% (v/v) penicillin streptomycin. All cell lines were cultured at 37 °C in a humidified incubator with 5% CO_2 (Eppendorf, Hamburg, Germany, 6731011515).

4.2. Isolation and culture of BMDMs

All primary cell harvest procedures were conducted in compliance with standards set by the Unit for Laboratory Animal Medicine (ULAM) with approval from the Institutional Animal Care and Use Committee (IACUC) of the University of Michigan. BMDMs were harvested from the tibial and femoral bone marrow of 8–12-week-old BALB/c mice and cultured in high glucose DMEM supplemented with 10% (v/v) FBS, 1% (v/v) penicillin streptomycin, and 1% (v/v) L-glutamine. Nonadherent cells were collected after a 24-h incubation period and differentiated with 20 ng/mL rM-MCSF for 8 days. Macrophage isolation was confirmed using flow cytometry to assess F4/80 expression on the cell surface [53].

4.3. NP formulation and characterization

Dye-loaded PLGA NPs were formulated via a single emulsion solvent evaporation process as outlined previously [4]. In brief, solid PLGA (50:50 lactide:glycolide) was dissolved in DCM at 50 mg/mL overnight. DiD (10 mg/mL in DMSO) was added to the polymer at 5 wt%. The polymer solution was added dropwise into 2 mL of 5% (*w/v*) PVA while vortexing to create an oil-in-water emulsion. The emulsion was then

sonicated three times at 38% amplitude for 10-s pulses (Sonics and Materials, Newtown, CT, VCX750). The sonicated solution was transferred into 10 mL of 0.3% (w/v) PVA and the remaining organic solvent was evaporated using a rotary evaporator (Buchi, New Castle, DE, Rotavapor R-100) at 70 mbar for 20 min. The remaining NP suspension was centrifuged at 18,000 x*g* for 15 min in a Sorvall X4 Pro-MD Centrifuge (ThermoFisher Scientific, Waltham, Massachusetts, 75016052). The supernatant was decanted, and the NP pellet was resuspended and sonicated in 10 mL Ultrapure water and centrifuged again at 18,000 x*g* for 15 min. This step was repeated to achieve a total of three washes. Hydrodynamic size and zeta potential of the resulting NP formulations were analyzed via DLS using a Malvern Zetasizer Advance - Ultra (Red) (Malvern Panalytical Ltd., Malvern, United Kingdom, ZSU3305).

Unloaded or blank PLGA decoy NPs were similarly formulated to achieve NP sizes of 200, 300, 400, and 500 nm. To achieve 300 nm NPs, a similar protocol was utilized; the only variation was during the sonication step, when the solution was instead sonicated for one 5-s pulse at 20% amplitude. Similarly, 400 nm NPs were formulated using a Cole-Palmer Ultrasonic Processor (Cole-Palmer, Vernon Hills, Illinois, EW-04714-50) for a single 10-s pulse at 20% amplitude and 500 nm for a single 5-s pulse at 20% amplitude. Finally, to formulate blank PEMA PLGA decoy NPs, the same protocol was followed except for the fact that 2% (*w/v*) PEMA was used in replacement for PVA and 1% (w/v) PEMA was used for the post-sonication dilution. For decoys used *in vivo*, the same protocol was used, however, DiD (10 mg/mL in DMSO) was added to the polymer at 5 wt%.

Dye-loaded PACE-PEG NPs were also formulated via a single emulsion solvent evaporation process. Solid PACE-PEG polymer (60 mol% 15-pentadecalonide (PDL)) was synthesized as described previously [48]. Similarly, PACE-PEG polymer was dissolved at 50 mg/mL in chloroform overnight [14]. After this step, the same protocol for PLGA NP formulation and characterization was followed barring NP washing by centrifugation. PACE-PEG NPs were centrifuged at 24,000 x*g* for 90 min twice.

4.4. Phagocytic activity assessment in cultured macrophages

RAW 264.7 cells were seeded at 200,000 cells/mL in 24-well tissue culture plates and BMDMs were seeded at 500,000 cell/mL in 24-well tissue culture plates. Cells were allowed to adhere for 24 h and were then treated with PLGA decoys. Blank NPs were formulated either with PVA or PEMA and administered to cells at a final concentration ranging from 0.05 mg/mL-0.4 mg/mL. After the allotted pre-treatment incubation period (4–48 h), the medium was aspirated and replaced with medium containing 0.05 mg/mL of DiD-loaded PLGA or PACE-PEG NPs for 24 h prior to harvest and analysis.

4.5. Flow cytometry analysis

Cells in 24-well tissue culture plates were washed with DPBS three times and then harvested via scraping. The cells were further washed via centrifugation at 135 RPM for 5 min two times and resuspended in 1× DPBS. After washing, the cells were resuspended in fluorescence activated sorting cell (FACS) buffer (2% w/v BSA in 1× DPBS). Flow Cytometry analysis was conducted on an Attune NXT 4 Laser Flow Cytometer (ThermoFisher, Waltham, MA). Data were analyzed using FlowJo™ v10.8 Software (BD Life Sciences, Franklin Lakes, New Jersey).

4.6. Fluorescence microscopy

To prepare for microscopy, cells were cultured in 24-well glass-bottom plates and washed with DPBS three times and then stained with Hoechst 33342 (10 mg/mL in DMSO stock) in culture medium at a volume ratio of 1:1000. After incubation with Hoechst for 20 min, the cells and fluorescent NPs were imaged on an EVOS M700 fluorescent microscope (ThermoFisher Scientific, Waltham, Massachusetts, AMF7000). For cargo-free PLGA NP decoy tracking studies, cell membranes were stained with DiO (10 mg/mL in DMSO stock) in culture medium at a volume ratio of 5:1000. After a 15-min incubation period, the cells were washed DPBS three times and then treated with the decoy of interest. The fluorescence intensity of NPs taken up by cells was quantified using a custom image processing MATLAB code described previously [17,42]. The fluorescent NP signal (fluorescence intensity) was normalized to nuclear signal.

4.7. Fluorescence quantification of cell culture medium

After incubation with therapeutic surrogate DiD-loaded PLGA NPs, 100 μL of conditioned medium was collected and added to 100 μL of DMSO. The DMSO-medium solution was left overnight to dissolve the PLGA polymer and release the dye from the NPs in solution. After 24 h, the fluorescence of the solution was measured on a fluorometer (DeNovix, Wilmington, DE, DS-11 FX+) as a measure of the number of NPs remaining in the medium (i.e. not phagocytosed by cells). A sample of DiD-loaded PLGA NPs was saved prior to treatment of cells and prepared in the same manner as a positive control. All fluorescence measurements were normalized with a medium-only blank.

4.8. In-vivo biodistribution of PLGA NP decoys and therapeutic surrogate PLGA NPs

All animal procedures were performed in accordance with the guidelines and policies of the University of Michigan's Unit for Laboratory Animal Medicine (ULAM) and approved by the Institutional Animal Care and Use Committee (IACUC) of the University of Michigan. Following federal guidelines, animals were housed in an environment with a 12 h light/12 h dark cycle, a temperature of 20–26 °C, and 30–70% humidity. Food and water were given ad libitum. 4–6-week-old BALB/c mice were administered a bolus 2 mg dose of DiD-loaded decoys via RO injection. Clodronate liposomes were administered at 2 mL/kg via RO injection. Four mice were used for each condition. Following a pre-treatment period of 24 h, mice were administered DiI-loaded PLGA NPs as a therapeutic surrogate NP for an additional 24 h via RO injection to achieve a blood concentration of 300 μg/mL. Proceeding treatment with DiI NPs, mice were euthanized via isoflurane overdose. After euthanasia, organs including the heart, liver, lung, spleen, kidneys, and bone marrow were harvested. Whole organ fluorescence of each tissue was imaged with an IVIS Spectrum (PerkinElmer, Waltham, MA, 124262) and quantified using Living Image v 4.7.4 software (PerkinElmer, Waltham, MA). Following imaging, organs were homogenized into single cell suspensions for analysis via flow cytometry. For processing of the liver and the lungs, each organ was manually sliced, added to 10 mL of enzyme solution (HBSS with 5 mg/mL Collagenase 1 and 1 mg/mL DNAse 1), and agitated for 30 min at 37 °C. After shaking, lung samples were further homogenized through an 18G needle. Both liver and lung cell slurries were filtered through a 70 μM cell strainer. Liver samples were washed with 30 mL of liver isolation buffer (4.8% (*w/v*) BSA and 2 mM EDTA in HBSS) and lung samples were washed with 5 mL 0.5% (w/v) BSA in PBS. Samples were centrifuged at 330 x*g* for 5 min, decanted, resuspended in 5 mL of PBS and spun again at the same settings. 2 mL of RBC lysis buffer was added to each sample for 2 min and quenched with 5 mL PBS and centrifuged again. Each pellet was resuspended in 100 μL of PBS with 1:1000 parts Hoechst for nuclear staining and 1:1000 parts Zombie Green for cell viability and incubated for 15 min at 4 °C. Samples were washed with 1 mL of FACS buffer (2% w/v BSA in PBS) and spun a final time. Final tissue pellets were resuspended in 500 μL FACS buffer before running on flow cytometry.

For processing of heart, spleen, and kidney tissues, each organ was homogenized into a single cell suspension through a 70 μM cell strainer. Cell slurries were collected in 5 mL of RPMI 1640 medium and

centrifuged at 330 x*g* for 5 min. The same protocol as outlined above for Hoechst and viability staining were repeated for these tissues. Finally, for processing of the bone marrow samples, the ends of each femur were carefully cut and the bone was flushed with 1 mL of RPMI 1640 medium. The samples were centrifuged at 330 x*g* for 5 min before being stained as outlined above. All samples were analyzed using an Attune NXT 4 Laser Flow Cytometer (ThermoFisher, Waltham, MA). Data were analyzed using FlowJo™ v10.8 Software (BD Life Sciences, Franklin Lakes, New Jersey).

4.9. Fluorescence microscopy of frozen liver and lung sections

A portion of harvested livers and lungs were embedded in OCT and sectioned into 10 μm thick slices with an QS12 cryostat (Avantik, Pine Brook, New Jersey). Liver sections were blocked with 10% goat serum in PBS for 50 min. After blocking incubation, the blocking buffer was removed, and the sections were washed with FACS buffer. Primary F4/80 antibody was added to sections at a concentration of 100 nM in FACS buffer and incubated for 50 min on ice. A liver section from mice that received no treatment was reserved for IgG isotype control staining which was treated at the same concentration as primary F4/80 antibody. After incubation with primary antibody or IgG isotype control, the sections were washed three times with FACS buffer. Secondary antibody (goat anti-mouse) was added to sections at a concentration of 133 nM in FACS buffer and incubated for another 50 min. Liver sections were washed an additional three times with PBS and left to dry for 15 min. 10 μL of Vectashield mounting medium was added to each section to mount a #1 coverslip before imaging on a EVOS M700 fluorescent microscope (ThermoFisher Scientific, Waltham, Massachusetts, AMF7000). The final wash step and mounting medium and coverslip application was performed for lung sections.

4.10. Cell viability assay

A CellTiter-Glo assay (Promega, Madison, WI, G7570) was used to assess cell viability via quantification of adenosine triphosphate (ATP) for all cargo-free PLGA decoy sizes (Fig. S4). Luminescence signal was measured and quantified with a BioTek Cytation 5 cell imaging multimode reader (BioTek, Winooski, VT).

4.11. Statistical analysis

All statistical analyses were performed using GraphPad Prism version 10 software (GraphPad, San Diego, CA). An ordinary one-way ANOVA with a Tukey's multiple comparisons post-test was used to analyze all data sets for statistical significance and calculate *p*-values. For all statistical tests, $P < 0.05$ was considered statistically significant.

Authors contribution

A.S.P. and P.M.P. designed and conceptualized project. P.M.P. developed methodology. P.M.P., A.G., M.E.S, A.I.M., and O.M.K. were responsible for investigation. P.M.P. conducted formal analysis of collected data. P.M.P drafted the initial manuscript with editing and consultation from A.S.P. A.S.P. was responsible for funding acquisition. All authors reviewed the final manuscript.

CRediT authorship contribution statement

Peyton M. Panovich: Writing – review & editing, Writing – original draft, Methodology, Investigation, Formal analysis, Conceptualization. **Aditi Ganesan:** Writing – review & editing, Investigation. **Arianna I. Markey:** Writing – review & editing, Investigation. **Miriam E. Stevens:** Writing – review & editing, Investigation. **Owen M. Kelly:** Writing – review & editing, Investigation. **Alexandra S. Piotrowski-Daspit:** Writing – review & editing, Writing – original draft, Supervision, Funding acquisition, Conceptualization.

Declaration of competing interest

The authors declare the following competing interests: A.S.P. is a founder of Xanadu Bio, Inc. A.S.P. is also an inventor on patent applications related to the work described here. The remaining authors declare no competing interests.

Acknowledgements

This work was supported by grants from the National Institutes of Health (NIH; R00 HL151806), the Cystic Fibrosis Foundation (CFF; PIOTRO21F5, HASTIN23G0-COLLAB), Emily's Entourage (Research Grant), and the PhRMA Foundation (Faculty Starter Grant in Drug Delivery) (all to A.S.P.).

Appendix A. Supplementary data

Supplementary data to this article can be found online at https://doi.org/10.1016/j.jconrel.2026.114699.

Data availability

The authors confirm that the data supporting the findings of this study are available within the article and its supplementary materials.

References

[1] L.R. Baden, H.M. El Sahly, B. Essink, K. Kotloff, S. Frey, R. Novak, D. Diemert, S. A. Spector, N. Rouphael, C.B. Creech, J. McGettigan, S. Khetan, N. Segall, J. Solis, A. Brosz, C. Fierro, H. Schwartz, K. Neuzil, L. Corey, P. Gilbert, H. Janes, D. Follmann, M. Marovich, J. Mascola, L. Polakowski, J. Ledgerwood, B.S. Graham, H. Bennett, R. Pajon, C. Knightly, B. Leav, W. Deng, H. Zhou, S. Han, M. Ivarsson, J. Miller, T. Zaks, Efficacy and safety of the mRNA-1273 SARS-CoV-2 vaccine, N. Engl. J. Med. 384 (2021) 403–416, https://doi.org/10.1056/nejmoa2035389.

[2] D. Adams, A. Gonzalez-Duarte, W.D. O'Riordan, C.-C. Yang, M. Ueda, A.V. Kristen, I. Tournev, H.H. Schmidt, T. Coelho, J.L. Berk, K.-P. Lin, G. Vita, S. Attarian, V. Planté-Bordeneuve, M.M. Mezei, J.M. Campistol, J. Buades, T.H. Brannagan, B. J. Kim, J. Oh, Y. Parman, Y. Sekijima, P.N. Hawkins, S.D. Solomon, M. Polydefkis, P.J. Dyck, P.J. Gandhi, S. Goyal, J. Chen, A.L. Strahs, S.V. Nochur, M.T. Sweetser, P.P. Garg, A.K. Vaishnaw, J.A. Gollob, O.B. Suhr, Patisiran, an RNAi therapeutic, for hereditary transthyretin amyloidosis, N. Engl. J. Med. 379 (2018) 11–21, https://doi.org/10.1056/nejmoa1716153.

[3] J.D. Gillmore, E. Gane, J. Taubel, J. Kao, M. Fontana, M.L. Maitland, J. Seitzer, D. O'Connell, K.R. Walsh, K. Wood, J. Phillips, Y. Xu, A. Amaral, A.P. Boyd, J. E. Cehelsky, M.D. McKee, A. Schiermeier, O. Harari, A. Murphy, C.A. Kyratsous, B. Zambrowicz, R. Soltys, D.E. Gutstein, J. Leonard, L. Sepp-Lorenzino, D. Lebwohl, CRISPR-Cas9 in vivo gene editing for transthyretin amyloidosis, N. Engl. J. Med. 385 (2021) 493–502, https://doi.org/10.1056/nejmoa2107454.

[4] A.S. Piotrowski-Daspit, A.C. Kauffman, L.G. Bracaglia, W.M. Saltzman, Polymeric vehicles for nucleic acid delivery, Adv. Drug Deliv. Rev. 156 (2020) 119–132, https://doi.org/10.1016/j.addr.2020.06.014.

[5] D.N. Kapoor, A. Bhatia, R. Kaur, R. Sharma, G. Kaur, S. Dhawan, PLGA: a unique polymer for drug delivery, Ther. Deliv. 6 (2015) 41–58, https://doi.org/10.4155/tde.14.91.

[6] S.N. Oyaghire, E. Quijano, A.S. Piotrowski-Daspit, W.M. Saltzman, P.M. Glazer, Poly(lactic-co-glycolic acid) nanoparticle delivery of peptide nucleic acids in vivo, in: Methods in Molecular Biology, Humana Press Inc., 2020, pp. 261–281, https://doi.org/10.1007/978-1-0716-0243-0_17.

[7] A.S. Piotrowski-Daspit, P.M. Glazer, W.M. Saltzman, Debugging the genetic code: non-viral in vivo delivery of therapeutic genome editing technologies, Curr. Opin. Biomed. Eng. 7 (2018) 24–32, https://doi.org/10.1016/j.cobme.2018.08.002.

[8] E. Saito, S.J. Gurczynski, K.R. Kramer, C.A. Wilke, S.D. Miller, B.B. Moore, L. D. Shea, Health and medicine modulating lung immune cells by pulmonary delivery of antigen-specific nanoparticles to treat autoimmune disease, Sci. Adv. (2020), https://doi.org/10.1126/sciadv.abc9317.

[9] K.R. Hughes, M.N. Saunders, J.J. Landers, K.W. Janczak, H. Turkistani, L.M. Rad, S. D. Miller, J.R. Podojil, L.D. Shea, J.J. O'Konek, Masked delivery of allergen in nanoparticles safely attenuates anaphylactic response in murine models of peanut allergy, Front. Allergy. 3 (2022), https://doi.org/10.3389/falgy.2022.829605.

[10] R. Putman, A.S. Ricciardi, K.E.W. Carufe, E. Quijano, R. Bahal, P.M. Glazer, W. M. Saltzman, Nanoparticle-mediated genome editing in single-cell embryos via peptide nucleic acids, Bioeng. Transl. Med. 8 (2023), https://doi.org/10.1002/btm2.10458.

[11] A.S. Piotrowski-Daspit, C. Barone, C.-Y. Lin, Y. Deng, D. Wu, T.C. Binns, E. Xu, A. S. Ricciardi, R. Putman, A. Garrison, R. Nguyen, A. Gupta, R. Fan, P.M. Glazer, W.

M. Saltzman, M.E. Egan, Health and medicine in vivo correction of cystic fibrosis mediated by PNA nanoparticles, Sci. Adv. (2022), https://doi.org/10.1126/sciadv.abo0522.
[12] J. Cui, L. Qin, J. Zhang, P. Abrahimi, H. Li, G. Li, G.T. Tietjen, G. Tellides, J. S. Pober, W. Mark Saltzman, Ex vivo pretreatment of human vessels with siRNA nanoparticles provides protein silencing in endothelial cells, Nat. Commun. 8 (2017), https://doi.org/10.1038/s41467-017-00297-x.
[13] J. Cui, A.S. Piotrowski-Daspit, J. Zhang, M. Shao, L.G. Bracaglia, T. Utsumi, Y. E. Seo, J. DiRito, E. Song, C. Wu, A. Inada, G.T. Tietjen, J.S. Pober, Y. Iwakiri, W. M. Saltzman, Poly(amine-co-ester) nanoparticles for effective Nogo-B knockdown in the liver, J. Control. Release 304 (2019) 259–267, https://doi.org/10.1016/j.jconrel.2019.04.044.
[14] A.S. Piotrowski-Daspit, L.G. Bracaglia, D.A. Eaton, O. Richfield, T.C. Binns, C. Albert, J. Gould, R.D. Mortlock, M.E. Egan, J.S. Pober, W.M. Saltzman, Enhancing in vivo cell and tissue targeting by modulation of polymer nanoparticles and macrophage decoys, Nat. Commun. 15 (2024), https://doi.org/10.1038/s41467-024-48442-7.
[15] Y.E. Seo, H.W. Suh, R. Bahal, A. Josowitz, J. Zhang, E. Song, J. Cui, S. Noorbakhsh, C. Jackson, T. Bu, A. Piotrowski-Daspit, R. Bindra, W.M. Saltzman, Nanoparticle-mediated intratumoral inhibition of miR-21 for improved survival in glioblastoma, Biomaterials 201 (2019) 87–98, https://doi.org/10.1016/j.biomaterials.2019.02.016.
[16] Y. Jiang, Q. Lu, Y. Wang, E. Xu, A. Ho, P. Singh, Y. Wang, Z. Jiang, F. Yang, G. T. Tietjen, P. Cresswell, W.M. Saltzman, Quantitating endosomal escape of a library of polymers for mRNA delivery, Nano Lett. 20 (2020) 1117–1123, https://doi.org/10.1021/acs.nanolett.9b04426.
[17] L.G. Bracaglia, A.S. Piotrowski-Daspit, C.-Y. Lin, Z.M. Moscato, Y. Wang, G. T. Tietjen, W.M. Saltzman, High-throughput quantitative microscopy-based half-life measurements of intravenously injected agents, PNAS (2020), https://doi.org/10.1073/pnas.1915450117/-/DCSupplemental.
[18] J. Lu, X. Gao, S. Wang, Y. He, X. Ma, T. Zhang, X. Liu, Advanced strategies to evade the mononuclear phagocyte system clearance of nanomaterials, Exploration 3 (2023) 20220045, https://doi.org/10.1002/exp.20220045.
[19] Y. Tang, X. Wang, J. Li, Y. Nie, G. Liao, Y. Yu, C. Li, Overcoming the reticuloendothelial system barrier to drug delivery with a "don't-eat-us" strategy, ACS Nano (2019), https://doi.org/10.1021/acsnano.9b05679.
[20] A.J. Tavares, W. Poon, Y.N. Zhang, Q. Dai, R. Besla, D. Ding, B. Ouyang, A. Li, J. Chen, G. Zheng, C. Robbins, W.C.W. Chan, C.J. Murphy, Effect of removing Kupffer cells on nanoparticle tumor delivery, Proc. Natl. Acad. Sci. USA 114 (2017) E10871–E10880, https://doi.org/10.1073/pnas.1713390114.
[21] D. Kurotaki, T. Uede, T. Tamura, Functions and development of red pulp macrophages, Microbiol. Immunol. 59 (2015) 55–62, https://doi.org/10.1111/1348-0421.12228.
[22] W. Poon, Y.N. Zhang, B. Ouyang, B.R. Kingston, J.L.Y. Wu, S. Wilhelm, W.C. W. Chan, Elimination pathways of nanoparticles, ACS Nano 13 (2019) 5785–5798, https://doi.org/10.1021/acsnano.9b01383.
[23] W. Ngo, S. Ahmed, C. Blackadar, B. Bussin, Q. Ji, S.M. Mladjenovic, Z. Sepahi, W.C. W. Chan, Why nanoparticles prefer liver macrophage cell uptake in vivo, Adv. Drug Deliv. Rev. 185 (2022), https://doi.org/10.1016/j.addr.2022.114238.
[24] K.M. Tsoi, S.A. Macparland, X.Z. Ma, V.N. Spetzler, J. Echeverri, B. Ouyang, S. M. Fadel, E.A. Sykes, N. Goldaracena, J.M. Kaths, J.B. Conneely, B.A. Alman, M. Selzner, M.A. Ostrowski, O.A. Adeyi, A. Zilman, I.D. McGilvray, W.C.W. Chan, Mechanism of hard-nanomaterial clearance by the liver, Nat. Mater. 15 (2016) 1212–1221, https://doi.org/10.1038/nmat4718.
[25] I.V. Zelepukin, K.G. Shevchenko, S.M. Deyev, Rediscovery of mononuclear phagocyte system blockade for nanoparticle drug delivery, Nat. Commun. 15 (2024), https://doi.org/10.1038/s41467-024-48838-5.
[26] S. Ravichandran, N. Manickam, M. Kandasamy, Liposome encapsulated clodronate mediated elimination of pathogenic macrophages and microglia: a promising pharmacological regime to defuse cytokine storm in COVID-19, Med. Drug Discov. 15 (2022), https://doi.org/10.1016/j.medidd.2022.100136.
[27] N.R.M. Saunders, M.S. Paolini, O.S. Fenton, L. Poul, J. Devalliere, F. Mpambani, A. Darmon, M. Bergère, O. Jibault, M. Germain, R. Langer, A Nanoprimer to improve the systemic delivery of siRNA and mRNA, Nano Lett. 20 (2020) 4264–4269, https://doi.org/10.1021/acs.nanolett.0c00752.
[28] M.P. Nikitin, I.V. Zelepukin, V.O. Shipunova, I.L. Sokolov, S.M. Deyev, P.I. Nikitin, Enhancement of the blood-circulation time and performance of nanomedicines via the forced clearance of erythrocytes, Nat. Biomed. Eng. 4 (2020) 717–731, https://doi.org/10.1038/s41551-020-0581-2.
[29] J. Wolfram, S. Nizzero, H. Liu, F. Li, G. Zhang, Z. Li, H. Shen, E. Blanco, M. Ferrari, A chloroquine-induced macrophage-preconditioning strategy for improved nanodelivery, Sci. Rep. 7 (2017), https://doi.org/10.1038/s41598-017-14221-2.
[30] A. Horatscheck, M. Krauß, H. Bulut, V. Chambon, M.S. Zadah, E. Dransart, K. Peloza, K.F. Santos, M.J. Robertson, K. Prichard, S. Miksche, S. Radetzki, J. P. von Kries, M.C. Wahl, A. McCluskey, L. Johannes, V. Haucke, M. Nazaré, Next-generation small molecule inhibitors of clathrin function acutely inhibit endocytosis, Structure (2025), https://doi.org/10.1016/j.str.2025.02.011.
[31] Z. Wan, L. Zhao, F. Lu, X. Gao, Y. Dong, Y. Zhao, M. Wei, G. Yang, C. Xing, L. Liu, Mononuclear phagocyte system blockade improves therapeutic exosome delivery to the myocardium, Theranostics 10 (2020) 218–230, https://doi.org/10.7150/thno.38198.
[32] A. Dirisala, S. Uchida, K. Toh, J. Li, S. Osawa, T.A. Tockary, X. Liu, S. Abbasi, K. Hayashi, Y. Mochida, S. Fukushima, H. Kinoh, K. Osada, K. Kataoka, Health and Medicine Transient Stealth Coating of Liver Sinusoidal Wall by Anchoring Two-Armed PEG for Retargeting Nanomedicines. https://www.science.org, 2020.
[33] C.N. Hess, C.C. Low Wang, W.R. Hiatt, Annual Review of Medicine PCSK9 Inhibitors: Mechanisms of Action, Metabolic Effects, and Clinical Outcomes 39, 2025 26, https://doi.org/10.1146/annurev-med-042716.
[34] A.L. Banka, M.V. Guevara, E.R. Brannon, N.Q. Nguyen, S. Song, G. Cady, D. J. Pinsky, K.E. Uhrich, R. Adili, M. Holinstat, O. Eniola-Adefeso, Cargo-free particles divert neutrophil-platelet aggregates to reduce thromboinflammation, Nat. Commun. 14 (2023), https://doi.org/10.1038/s41467-023-37990-z.
[35] Y. Zhang, K.R. Hughes, R.M. Raghani, J. Ma, S. Orbach, J.S. Jeruss, L.D. Shea, Cargo-free immunomodulatory nanoparticles combined with anti-PD-1 antibody for treating metastatic breast cancer, Biomaterials 269 (2021), https://doi.org/10.1016/j.biomaterials.2021.120666.
[36] L.M. Casey, S. Kakade, J.T. Decker, J.A. Rose, K. Deans, L.D. Shea, R.M. Pearson, Cargo-less nanoparticles program innate immune cell responses to toll-like receptor activation, Biomaterials 218 (2019), https://doi.org/10.1016/j.biomaterials.2019.119333.
[37] S. Chen, A.F.U.H. Saeed, Q. Liu, Q. Jiang, H. Xu, G.G. Xiao, L. Rao, Y. Duo, Macrophages in immunoregulation and therapeutics, Signal Transduct. Target. Ther. 8 (2023), https://doi.org/10.1038/s41392-023-01452-1.
[38] T. Bleul, X. Zhuang, A. Hildebrand, C. Lange, D. Böhringer, G. Schlunck, T. Reinhard, T. Lapp, Different innate immune responses in BALB/c and C57BL/6 strains following corneal transplantation, J. Innate Immun. 13 (2021) 49–59, https://doi.org/10.1159/000509716.
[39] U. Jaggi, M. Yang, H.H. Matundan, S. Hirose, P.K. Shah, B.G. Sharifi, H. Ghiasi, Increased phagocytosis in the presence of enhanced M2-like macrophage responses correlates with increased primary and latent HSV-1 infection, PLoS Pathog. 16 (2020), https://doi.org/10.1371/journal.ppat.1008971.
[40] H.K. Mandl, E. Quijano, H.W. Suh, E. Sparago, S. Oeck, M. Grun, P.M. Glazer, W. M. Saltzman, Optimizing biodegradable nanoparticle size for tissue-specific delivery, J. Control. Release 314 (2019) 92–101, https://doi.org/10.1016/j.jconrel.2019.09.020.
[41] B. Li, L. Ma, X. Li, Z. Suleman, C. Liu, O. Piskareva, M. Liu, Size matters: altering antigen specific immune tolerance by tuning size of particles, J. Control. Release 373 (2024) 823–836, https://doi.org/10.1016/j.jconrel.2024.07.077.
[42] C. Albert, L. Bracaglia, A. Koide, J. DiRito, T. Lysyy, L. Harkins, C. Edwards, O. Richfield, J. Grundler, K. Zhou, E. Denbaum, G. Ketavarapu, T. Hattori, S. Perincheri, J. Langford, A. Feizi, D. Haakinson, S.A. Hosgood, M.L. Nicholson, J. S. Pober, W.M. Saltzman, S. Koide, G.T. Tietjen, Monobody adapter for functional antibody display on nanoparticles for adaptable targeted delivery applications, Nat. Commun. 13 (2022), https://doi.org/10.1038/s41467-022-33490-8.
[43] R. Bahal, N. Ali McNeer, E. Quijano, Y. Liu, P. Sulkowski, A. Turchick, Y.C. Lu, D. C. Bhunia, A. Manna, D.L. Greiner, M.A. Brehm, C.J. Cheng, F. López-Giráldez, A. Ricciardi, J. Beloor, D.S. Krause, P. Kumar, P.G. Gallagher, D.T. Braddock, W. Mark Saltzman, D.H. Ly, P.M. Glazer, In vivo correction of anaemia in β-thalassemic mice by γ3PNA-mediated gene editing with nanoparticle delivery, Nat. Commun. 7 (2016), https://doi.org/10.1038/ncomms13304.
[44] P.M. Panovich, A. Ganesan, A.R. Angadi, A.S. Piotrowski-Daspit, Recent advances in the application of polymeric nanoparticles to the pulmonary delivery of mRNA, Nanomedicine (2025), https://doi.org/10.1080/17435889.2025.2509477.
[45] C.A. Hodges, R.A. Conlon, Delivering on the promise of gene editing for cystic fibrosis, Genes Dis. 6 (2019) 97–108, https://doi.org/10.1016/j.gendis.2018.11.005.
[46] N.E. Allaire, U. Griesenbach, B. Kerem, J.D. Lueck, N. Stanleigh, Y.S. Oren, Gene, RNA, and ASO-based therapeutic approaches in cystic fibrosis, J. Cyst. Fibros. 22 (2023) S39–S44, https://doi.org/10.1016/j.jcf.2022.12.016.
[47] M.K. Grun, A. Suberi, K. Shin, T. Lee, V. Gomerdinger, Z.M. Moscato, A. S. Piotrowski-Daspit, W.M. Saltzman, PEGylation of poly(amine-co-ester) polyplexes for tunable gene delivery, Biomaterials 272 (2021), https://doi.org/10.1016/j.biomaterials.2021.120780.
[48] A.C. Kauffman, A.S. Piotrowski-Daspit, K.H. Nakazawa, Y. Jiang, A. Datye, W. M. Saltzman, Tunability of biodegradable poly(amine- co-ester) polymers for customized nucleic acid delivery and other biomedical applications, Biomacromolecules 19 (2018) 3861–3873, https://doi.org/10.1021/acs.biomac.8b00997.
[49] A.K. Patel, J.C. Kaczmarek, S. Bose, K.J. Kauffman, F. Mir, M.W. Heartlein, F. DeRosa, R. Langer, D.G. Anderson, Inhaled nanoformulated mRNA Polyplexes for protein production in lung epithelium, Adv. Mater. 31 (2019), https://doi.org/10.1002/adma.201805116.
[50] E.L. Blanchard, D. Vanover, S.S. Bawage, P.M. Tiwari, L. Rotolo, J. Beyersdorf, H. E. Peck, N.C. Bruno, R. Hincapie, F. Michel, J. Murray, H. Sadhwani, B. Vanderheyden, M.G. Finn, M.A. Brinton, E.R. Lafontaine, R.J. Hogan, C. Zurla, P. J. Santangelo, Treatment of influenza and SARS-CoV-2 infections via mRNA-encoded Cas13a in rodents, Nat. Biotechnol. 39 (2021) 717–726, https://doi.org/10.1038/s41587-021-00822-w.
[51] Y. Wang, B. Qin, G. Xia, S.H. Choi, FDA'S poly (lactic-co-glycolic acid) research program and regulatory outcomes, AAPS J. 23 (2021), https://doi.org/10.1208/s12248-021-00611-y.
[52] D. Horvath, M. Basler, PLGA particles in immunotherapy, Pharmaceutics 15 (2023), https://doi.org/10.3390/pharmaceutics15020615.
[53] E.M. Bruscia, P.X. Zhang, E. Ferreira, C. Caputo, J.W. Emerson, D. Tuck, D. S. Krause, M.E. Egan, Macrophages directly contribute to the exaggerated inflammatory response in cystic fibrosis transmembrane conductance regulator−/−mice, Am. J. Respir. Cell Mol. Biol. 40 (2009) 295–304, https://doi.org/10.1165/rcmb.2008-0170OC.

Glossary

ATP: adenosine triphosphate
BMDM: Bone Marrow Derived Macrophages
BSA: Bovine Serum Albumin
CF: Cystic Fibrosis
CFTR: Cystic Fibrosis Transmembrane Conductance Regulator
COPD: Chronic Obstructive Pulmonary Disease
DCM: Dichloromethane
DiD: DiIC18(5) 1,1′-dioctadecyl-3,3,3′,3′-tetremethylindodicarboyanine, 4-chlorobenzenesulfonate salt
DiI: $DiIC_{18}(3)$ 1,1′-dioctadecyl-3,3,3′,3′, tetramethylindocarbocyanine
DMEM: Dulbecco's Modified Eagle's Medium
DMSO: Dimethyl Sulfoxide
DLS: Dynamic Light Scattering
DiO: Benzoxazolium 3-octadecyl-2-[3-(3-octadecyl-2(3H)-benzoxazolylidene)-1-propenyl]-perchlorate
DPBS: Dulbecco's Phosphate Buffered Saline
EDTA: ethylenediaminetetraacetic acid
FACS: Fluorescence Activated Cell Sorting
FBS: Fetal Bovine Serum
HBSS: Hank's Balanced Salt Solution
IACUC: Institutional Animal Care and Use Committee
ILD: Interstitial Lung Disease
IV: Intravenous
IVIS: In-Vivo Imaging System
LDL: Low Density Lipoprotein
LNP: Lipid Nanoparticle
MFI: Mean Fluorescence Intensity
MPS: Mononuclear Phagocytic System
NP: Nanoparticle
OCT: Optimal Cutting Temperature
PACE: Poly(amine-co-ester)
PBAE: Poly(beta-amino ester)
PCSK9: Proprotein Convertase Subtilisin/Kexin Type 9
PDL: 15-pentadecalonide
PEG: Poly(ethylene glycol)
PEMA: Poly(ethylene-*alt*-maleic-anhydride)
PLGA: Poly(lactic-co-glycolic acid)
PNA: Peptide Nucleic Acid
PVA: Poly(vinyl alcohol)
RFU: Relative Fluorescence Intensity
rM-MCSF: Recombinant Mouse Macrophage Colony Stimulating Factor
RO: Retro-Orbital
RPMI: Roswell Park Memorial Institute
ULAM: Unit for Laboratory Animal Medicine